CWP-262
ACTI, 4731U0015-2F
August, 1997

True Amplitude Transformation to Zero Offset of Data from Curved Reflectors

Norman Bleistein, Jack K. Cohen and
Herman Jaramillo

This is a report for ACTI Project, No. 4731U0015-2F, submitted to Los Alamos National Laboratory and industry project partners, August, 1997. This research is also partially supported by the Center for Wave Phenomena Consortium Project at the Colorado School of Mines. This report significantly extends the research reported to the sponsors in CWP-193, November, 1995.

Center for Wave Phenomena
Colorado School of Mines
Golden, Colorado 80401
303/273-3557

ABSTRACT

Transformation to zero offset (TZO), alternatively known as migration to zero offset (MZO), or the combination of normal moveout and dip moveout (NMO/DMO), is a process that transforms data collected at finite offset between source and receiver to a pseudo zero offset trace. The kinematic validity of DMO processing has been well established. Furthermore, the dynamical validity for planar reflectors has been established in earlier studies, as well. This means that the traveltime and geometrical spreading terms of the finite offset data are transformed to their counterparts for zero offset data, while the finite offset reflection coefficient is preserved.

The purpose of this study is to extend the dynamical validity to the case of curved reflectors in the two-and-one-half dimensionsal limit. That is, we show that the amplitude factor attributed to curvature effects in finite offset data is transformed by this processing to the corresponding curvature factor for zero offset data.

This problem has also been addressed in a more general context by Tygel, etal, 1997. However, in the generality, some of the specifics and interpretations of the simpler problem are lost. Thus, we see some value in presenting this analysis where one carry out all calculations explicitly and see specific quantities that are more familiar and accessible to users of DMO.

Fruthermore, in this paper, we also show how processing a second DMO operator allows for the extraction of the cosine of the preserved specular angle, a necessary piece of information for *amplitude versus angle* (AVA) analysis. We then discuss the possibility of using the output of our processing formalism at multiple offsets to create a table of angularly dependent reflection coefficient and attendant incidence angle as a function of offset. This is the basis of a proposed AVO/AVA analysis of the pseudo zero offset traces.

INTRODUCTION

Transformation to zero offset (TZO), alternatively known as migration to zero offset (MZO), or the combination of normal moveout and dip moveout (NMO/DMO), is a technique for preprocessing traces of data at finite offset to produce a *pseudo zero offset* data set. In this study, we consider TZO processing for a common (fixed) offset data set in an acoustic medium with constant background propagation speed.

Current formalisms adequately map the arrival times of reflection "events" in the transformed data set—the kinematics of the data set—but analysis of the effect of this processing on amplitude—the dynamics—of the data set has been incomplete until recently. That is, given model data at finite offset, earlier work Liner [1990, 1991], Bleistein [1990], Black, et al [1993], Zhang [1988], have provided an adequate analysis

for the case of analytical model data for a horizontal or dipping planar reflector. However, the analysis of the effect of curvature of the reflector on the output of TZO processing is the main subject of this paper.

Another approach to this problem is provided by Tygel, et al, [1995b]. This work is based on the theory presented in an earlier paper, Tygel, et al [1995a], in which the curvature of isochrons plays a crucial role in the analysis and interpretation of the wave propagation. Their method is general and powerful; indeed, it has motivated further research in our own group. However, some easily interpretable features of the specific case—constant background TZO—are lost in the generality of their approach; hence, the point of presenting this simpler analysis and derivation.

Furthermore, we present results not present in their work. One such result is a technique for estimating the angle of incidence associated with the preserved finite offset specular reflection coefficient. The method is straightforward; we need only process two TZO operators simultaneously. The two differ in an amplitude factor whose value requires little additional computation. The quotient of peak values of these two outputs yields an estimate of the cosine of the specular angle. It is important to note that this technique does not rely on the true amplitude nature of the TZO operator, but only on the two kernels differing by a factor derived below. Thus, this attribute is attainable with any standard integral DMO processing.

A second new result is an approach to AVO/AVA analysis of the transformed data. Data from all offsets map to zero offset data with identical geometrical spreading effects, differing only in that the reflection coefficient of the original offset is preserved in the amplitude. Thus, by stripping away the geometrical spreading effects at peak amplitude, only the offset dependent reflection coefficient remains. That is, we can tabulate the reflection coefficient of an event as a function of offset. Thus, we have data for AVO analysis. However, as noted above, we can also determine the specular incidence angle as a function of offset. Thus, we can generate a three column table, in which the first column is offset, the second is specular reflection coefficient of an event of the input data and the third is the specular incidence angle of that reflection coefficient. The use of the last two columns provides data for AVA analysis. This is AVA.

For all of these results, our primary form of transformation is from space/frequency domain to space/frequency domain. However, we also present a Hale-type TZO—a true amplitude analog of Hale DMO [1984]—and a Gardner/Forel [1988, 1995] TZO, along with the necessary additional operators required to extract the cosine of the incidence angle for these two alternative TZO formalisms. While the Hale TZO has been presented earlier [Bleistein, 1990], the Gardner/Forel TZO has not. Furthermore, the operators for determining the cosine of the specular angle for both of these forms of DMO are new. In fact, we used the Hale TZO for our numerical tests. That is, we modified the amplitude in that code as indicated below to provide a true amplitude TZO from which to test our predicted output amplitude. Then, we introduced the appropriate multiplier to produce the second output, differing from the first by a factor

of cosine of the specular angle. The numerical tests confirm our theory and confirm the asymptotic equivalence of the true amplitude TZO operators.

We note that a third approach to the transformation problem has been pursued by Fomel [1995a, 1995b] and Fomel, et al [1996], in the context of a more general *offset continuation* analysis. That method is based on a kinematically derived wave equation in offset, midpoint and time. Thus, by the nature of its derivation, it properly predicts the transformation of traveltime. In fact, when specialized to zero offset, this approach predicts the same amplitude result as we obtain here. The derivation based on kinematics alone—essentially, a differential equation for wave propagation predicted from a dispersion relation—is not guaranteed to predict a "correct" amplitude. However, the result of Fomel, et al, [1996] is that this offset continuation method does, indeed, predict amplitude transformation accurately, as well. That is, Fomel's offset continuation via a differential equation produces the same transformation of curvature effect from finite offset to zero offset as does the formalism presented here.

The processing formula we derive here is the result of cascading an inversion formula—to derive an earth model from the common offset data—with a modeling formula—to derive a zero offset data set from the derived earth model. Both processes are integrals. The former is an integral over the input variables of the data set (time and midpoint, or frequency and midpoint, or frequency and midpoint wave number, or time and midpoint wave number); the latter process is an integral over the spatial coordinates of the model. The result of this cascade is to produce an output in any of the types of variables listed previously for the input. Neither the input data nor the output data of the cascaded processes depend on the model variables; only the cascaded operators depends on those. Thus, the integrations in those spatial variables can be carried out asymptotically to deduce a processing formula to map the finite offset data to a zero offset data set, solely as an integral over the input variables.

In our approach, there are five main constituents to geometrical optics data:

1. the phase, consisting of the frequency multiplying the two way traveltime from source to reflector to receiver on a specular ray path—plus, perhaps, a phase shift term to account for caustics (buried foci);

2. the geometrical optics reflection coefficient at the specular incidence angle;

3. the source signature;

4. an amplitude factor characterizing geometrical spreading based only on the dip of the reflector—a multiplier that is the same for planar or curved reflectors;

5. a multiplier to account for the geometrical spreading effect due to curvature of the reflector.

In the analysis of Tygel, et al, [1995a, 1995b, 1997], the description of the amplitude in the last two items has to be modified. They prefer a "point scatterer"

description, in which the geometrical spreading effects are broken into three terms, namely, point source spreading from the source, point source spreading from the receiver and everything else. This description of the amplitude is natural if one starts from the Kirchhoff integral representation of the modeling problem; ours is more natural if one starts from ray theory, building up the amplitude as products and quotients of Jacobians, one from the source, another from the reflection process.

Since all analyses previous to ours and Tygel, et al, dealt with planar reflectors, the transformation via TZO processing of the finite offset curvature effect has not previously been analyzed for these types of integral formalisms. Here, in summary, are the known results for the first four effects.

1. The finite offset traveltime is mapped to the zero offset traveltime.

2. The finite offset reflection coefficient is preserved and *not* replaced by the zero offset reflection coefficient. More precisely, the zero offset ray shares the specular point with one[1] finite offset source/receiver pair. The reflection coefficient at the incidence angle of that specular source/receiver pair is preserved.

3. The bandwidth of the source is scaled by the cosine of the incidence angle and the source signature in the frequency domain is compressed into that smaller bandwidth. We remark that the compression in the frequency domain leads to the same resolution on spatial output for the migration/inversion of the finite offset data as for the mapped zero offset data.

4. The finite offset geometrical spreading that characterizes the dip of the reflector, alone, is mapped to the corresponding zero offset geometrical spreading.

The new result of this paper deals with the last item of our constituent list. We find that the finite offset geometrical spreading effect due to curvature of the reflector is mapped to the zero offset geometrical spreading effect. In fact, calling this a "spreading effect" is somewhat misleading; it is *spreading* when the reflector is convex-up, but it is *compressing* when the reflector is convex-down.

Two-and-one-half dimensional.

The formulas that we use for inversion and modeling are *two-and-one-half dimensional* (2.5D). This is a descriptive term for our approach to coping with a single line of data over a three-dimensional earth. We suppose that there are no variations in the out-of-plane direction below the vertical plane determined by the line of data. In this case, every parallel line of data would be exactly the same. Thus, having gathered one line of data, one has actually carried out an areal survey along parallel lines. Of course, we do not believe that the subsurface actually has this structure, but it is

[1] maybe more than one for a curved reflector

often approximately true and it seems to us that we can do no better with a classical single-line survey.

Conveniently, we have a 3D inversion formula that can process this type of common offset data on parallel lines. For the case under consideration, only the operator kernel depends on the out-of-plane variable; the data does not. Therefore, the out-of-plane integration can be computed in advance, leaving an inversion formalism that requires only an integration over the line where the data was gathered.

This is a specialization of a 3D inversion formula. Hence, it includes 3D propagation effects in determining a 2D velocity perturbation. It is this hybrid 3D/2D character that has led to the designation, 2.5D.

The Born approximation.

Both our inversion formula and our modeling formula are based on the Born approximation, which is a small perturbation approximation. The bandlimited nature of the data and the experiments we do suggests that we should primarily look for the reflectors in the earth, as opposed to seeking the slow variations of earth parameters by these methods. Because of the use of perturbation theory, one would expect the resulting formalism to be valid only for small perturbations in earth parameters. However, we have found a way to extend our results beyond the limit of the small perturbation assumption. To do this, we apply our results to geometrical optics data or Kirchhoff approximate data. These are high frequency models, not restricted to small perturbations in parameters across reflectors. For our inversion formalism, we use asymptotic analysis on the application of our integral operators to these high frequency data. What we find is that the output is actually linear in the geometrical optics reflection coefficient, rather than linear in the perturbation.

This interpretation in terms of Kirchhoff approximate data dramatically extends the range of validity of our inversion formalism. The reflection coefficient is not restricted to small changes in earth parameters across the reflector. Thus, if we adequately describe the medium above the reflector, the inversion not only locates the reflector accurately, but it also provides a good estimate of the reflection coefficient at some distinguished incidence angle with respect to the normal. Further, we can extend the method to estimate that incidence angle, as well as other parameters of the geometry of the source/receiver ray trajectories to the reflection point [Geoltrain, 1991].

The "distinguished angle" is the one for which the geometrical optics ray pair from source and receiver to reflection point are specular at the reflection point. An important feature of this processing is that we can determine this distinguished angle without determining the distinguished source and receiver positions. However, those are determinable, as well.

We repeat this type of analysis here. That is, we apply our TZO formalism to Kirchhoff approximate data for a single curved reflector. Furthermore, the same "trick" as we use in inversion to identify the specular angle will be used here to

determine the preserved incidence angle of the reflection coefficient after TZO processing.

We explain our results in more detail with the aid of Figure 1. In this figure, the

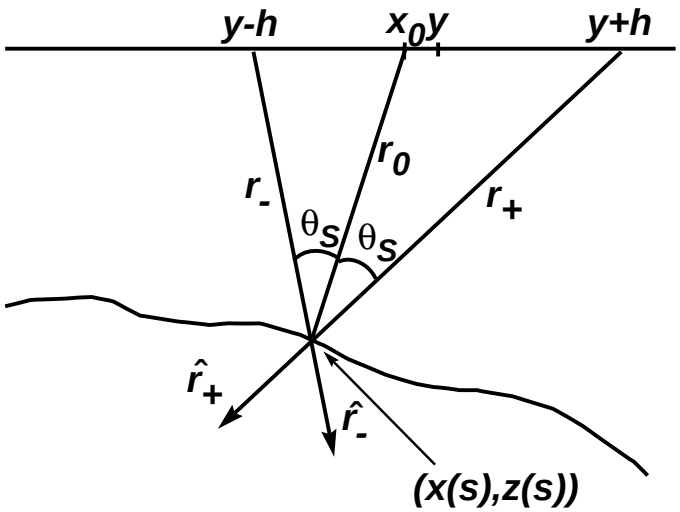

FIG. 1. Specular geometry for TZO processing.

zero offset point x_0 and the finite offset source/receiver pair, $y \mp h$, share the same specular point, $(x(s), z(s))$. For a single specular point where the reflector is convex up[2] as shown in the figure, the finite offset reflection data is given asymptotically by

$$u(y,\omega,h) = \frac{F(\omega)R(\cos\theta_S)}{4\pi(r_+ + r_-)}\sqrt{\frac{\rho_0\cos^2\theta_S}{r_0+\rho_0\cos^2\theta_S}}\exp\{i\omega(r_+ + r_-)/c\}. \tag{1}$$

In this equation, $F(\omega)$ is the source signature and $R(\cos\theta_S)$ is the geometrical optics reflection coefficient at incidence angle θ_S. In the context of our list above, $(r_+ + r_-)/c$ is the traveltime from source to reflector to receiver at propagation speed c; the factor, $1/(r_+ + r_-)$ is the planar geometrical spreading depending on the dip of the reflector, only, while the factor,

$$\sqrt{\frac{\rho_0\cos^2\theta_S}{r_0+\rho_0\cos^2\theta_S}},$$

is the spreading effect due to curvature; ρ_0 is the radius of curvature at the specular point of the cross sectional curve that defines the reflecting surface.

The corresponding zero offset data is

$$u(x_0,\omega,0) = \frac{F(\omega)R_n}{8\pi r_0}\sqrt{\frac{\rho_0}{r_0+\rho_0}}\exp\{2i\omega r_0/c\}. \tag{2}$$

Here, we use the notation $R_n = R(\cos 0) = R(1)$ for the zero offset (normal incidence) reflection coefficient. The two-way traveltime is now $2r_0/c$ and the geometrical dip

[2]This restriction is removed in the text. Here, this case is discussed for ease of exposition.

spreading effect is now $2r_0$. Note that the effect of curvature at finite offset is expressed in terms of r_0, the zero offset distance to the reflector, and that this curvature effect factor differs from the zero offset curvature effect factor only in that the *effective* radius of curvature is $\rho_0 \cos^2 \theta_S$ in the finite offset case.

We find that the output of our TZO processing is

$$u_0(x_0, \omega_0) = \frac{F(\omega_0 \sec \theta_S) R(\cos \theta_S)}{8\pi r_0} \sqrt{\frac{\rho_0}{r_0 + \rho_0}} \exp\{2i\omega r_0/c\}. \tag{3}$$

A comparison of equations (1), (2) and (3) will confirm the list of features of the TZO processing outlined above. For planar reflectors, one need only take the limit as $\rho_0 \to \infty$ in all three equations above to obtain the corresponding results; that is, replace the geometrical curvature factor by unity in each formula. The traveltime transformation, the geometrical spreading dependence on dip, and the preservation of the angularly dependent reflection coefficient by TZO are as expressed in equations (1) and (3). Thus, the earlier results are subsumed under the more general results presented in this paper.

We note that in (3), the frequency of the source signature has been scaled by $\sec \theta_S$. We remark that this is exactly the right scaling factor to preserve resolution after migration/inversion. The reason is that the normal wave number of the prestack migration/inversion is proportional to the bandwidth scaled by $\cos \theta_S$, whereas for zero offset migration/inversion it is proportional to the bandwidth. Hence, if the bandwidth were not scaled down by the TZO processing, the resolution after TZO would be higher than it was before. That cannot happen. The sampling information in the data cannot be changed by these linear processes.

It is useful to write down the result of transforming (3) back to the time domain:

$$U_0(x_0, t_0) = \frac{R(\cos \theta_S)}{8\pi r_0} \sqrt{\frac{\rho_0}{r_0 + \rho_0}} \int F(\omega_0 \sec \theta_S) \exp\{2i\omega r_0/c - \omega_0 t_0\} d\omega_0. \tag{4}$$

Note that the peak value of this output is

$$\begin{aligned} U_{0PEAK} &= \frac{R(\cos \theta_S)}{8\pi r_0} \sqrt{\frac{\rho_0}{r_0 + \rho_0}} \int F(\omega_0 \sec \theta_S) d\omega_0 \\ &= \frac{R(\cos \theta_S)}{8\pi r_0} \sqrt{\frac{\rho_0}{r_0 + \rho_0}} \cos \theta_S \int F(\omega) d\omega. \end{aligned} \tag{5}$$

It is this result that will become the basis for our proposed AVO/AVA analysis.

We noted above that there are choices of input variables and output variables to be made in developing a TZO formula. For theoretical purposes, we prefer to analyze the transformation from space/frequency input data to space/frequency output

data. That is because the asymptotic modeling data that we use is expressed in these variables. Thus, the TZO formula derived here is

$$u_0(x_0,\omega_0) = \frac{h^2}{\pi c}\int_{x_0-h}^{x_0+h} dy \int_{\nu\geq 1} d\omega\, \nu \exp\{i\omega_0\Phi_0/c\}\cdot\left[\frac{2h^2}{P^2}-1\right]\cdot\frac{u(y,\omega,h)}{p^2}. \tag{6}$$

In this equation,

$$\begin{aligned} \Phi_0 &= -2p, \qquad & p &= \sqrt{(x_0-y)^2+(\nu^2-1)h^2}, \\ P &= \sqrt{h^2-(x_0-y)^2}, \qquad & \nu &= \omega/\omega_0. \end{aligned} \tag{7}$$

The apparent singularity here at $y = x_0 \pm h$ is discussed below.

In the next section, we derive this TZO formula. The derivation leads to a mapping of common offset data in the spatial/frequency domain to zero offset data in the spatial/frequency domain. The rescaling of frequency is a natural outcome of that derivation. We also present in that section our counterpart to Hale's NMO/DMO, mapping wave number/temporal data to spatial/frequency data.

For Hale NMO/DMO, we need to express $u_0(x_0,\omega_0)$ in terms of the observed data in the (k,t)-domain. To derive that result from (6), we first set

$$u(y,\omega,h) = \frac{1}{2\pi}\int dk\; dt U(k,t,h)\exp\{i(ky+\omega t)\}. \tag{8}$$

This result is substituted into (6). Now the data does not depend on ω or y and those two integrals can be carried out by the method of stationary phase. The result is

$$u_0(x_0,\omega_0) = \frac{1}{2\pi}\int \frac{dk\; dt_n}{A}\left[1+\frac{2k^2h^2}{\omega_0^2 t_n^2}\right]U(k,t,h)\exp\{i\Theta\}. \tag{9}$$

In this equation,

$$t_n = \sqrt{t^2-(2h/c)^2}, \quad A = \sqrt{1+(kh/\omega_0 t_n)^2}, \quad \Theta = kx_0+\omega_0 t_n A \tag{10}$$

The result (9) differs from Hale's through the factor in square braces under the integral sign. The differences in alternative forms of Hale-type processing have been discussed in other papers, such as Black, et al [1993] and Fomel [1995b]. This integrand has a singularity at $t = 2h/c$. In fact, this corresponds to the singularity at $y = x_0 \pm h$, above. However, for reasons discussed below, we can be assured that the reflection data, U, itself, is zero near there and, hence, the total integrand is not singular in this limit. As a practical matter, we simply mute the traces for data near this travel time. We remark that the NMO component of this processing amounts to using (10) to evaluate t in (9).

Similar to our derivation of a Hale NMO/DMO, we can derive a transformation from space/time data to space/time data of the type proposed by Gardner and Forel

[1988, 1995]. We do this by taking the Fourier transform of the result in (6) from ω_0 to t_0 and then carrying out the integration in ω_0 by the method of stationary phase. The result is

$$U_0(x_0,t_0) = ht_0\sqrt{\frac{ch}{\pi}}\int_{x_0-h}^{x_0+h} dy \frac{D_{1/2}[u;t]}{P^{5/2}\left(c^2t_0^2+4P^2\right)^{1/4}}\left[\frac{2h^2}{P^2}-1\right]. \tag{11}$$

In this equation,

$$D_{1/2}[u;t] = \frac{1}{2\pi}\int d\omega\ \sqrt{|\omega|}\ \exp\{i\pi/4\ \mathrm{sgn}(\omega) - i\omega t\}u(y,\omega) \tag{12}$$

and

$$t = \frac{h}{cP}\sqrt{4P^2+c^2t_0^2}. \tag{13}$$

We remark that, if the filter in the operator, $D_{1/2}$ were $\exp\{-i\pi/4\ \mathrm{sgn}(\omega)\}$, then this operator would be just the *half derivative* of the data traces. The given operator is the product of that filter with the filter, $\exp\{i\pi/2\ \mathrm{sgn}(\omega)\} = i\mathrm{sgn}(\omega)$, which is the Fourier transform of $1/t$, within a scale. Hence, $D_{1/2}$ may be thought of as the half derivative of the *Hilbert transform* of the data.

In any case, the formula requires that we first filter all of the traces as in (12), and then perform the weight sum over midpoints, with the data on each trace being evaluated at the time indicated in (13).

The definition of t in (13) defines the evaluation time for this formalism to be as predicted in Gardner and Forel's DMO. However, those authors predict an amplitude that is just a stretch by $\sqrt{t_0}$ which is not the same as the result predicted here.

In the section following the derivation, we introduce Kirchhoff approximate data for a single reflector and derive the geometrical optics data, explaining along the way some special issues with which one must be concerned.

With the derivation of our TZO formula in place and the modeling data introduced, we then turn in the following section to the check of our formula on the model data. That is, we describe the application of our formalism to ray data for a dipping planar reflector—as a "warm-up"—and then apply our formula to to Kirchhoff data from a single curved reflector and derive the result presented in equation (3), above. We do this for the space/frequency to space/frequency mapping. However, the asymptotic equivalence of all the forms of TZO assures us that the same result is true for any of the mappings.

As an outgrowth of this last discussion, we are able to show how, at little additional CPU cost, one can simultaneously obtain an estimate of the cosine of the specular angle of the preserved reflection coefficient. One needs only to keep two running sums whose summands differ in one factor. The ratio of the two outputs then gives the unknown cosine. Having this value facilitates AVA study from our processing.

Let us denote the second TZO outputs as u_1 or U_1 in the appropriate variables. Then the modification of the formula (6) to produce this second output is as follows:

$$u_1(x_0,\omega_0) = \frac{h^2}{\pi c}\int_{x_0-h}^{x_0+h} dy \int_{\nu\geq 1} \nu^2 d\omega\ \exp\{i\omega_0\Phi_0/c\}\cdot\left[\frac{2h^2}{P^2}-1\right]\cdot\frac{u(y,\omega,h)}{p^2}. \tag{14}$$

That is, we need only multiply the previous operator amplitude by ν to obtain an output that, at peak amplitude, differs from the former by the secant of the specular angle of the input data. We do not need to know anything about the reflector or the specular reflection that produced the data. The key to obtaining this result is the asymptotic analysis of model data. What we find from that analysis is that the stationary value of ν is exactly $\sec\theta_S$, the secant of the angle of incidence of the specular reflection that produced the peak on the data trace. This is implicit in the result, (3), in the scaling of the source signature. We also see in the peak amplitude in (5), that there is a "natural" multiplier of $\cos\theta_S$ in the output. Thus, the revised operator simply removes that factor in the peak amplitude and the ratio, U_{0PEAK}/U_{1PEAK} will be just $\cos\theta_S$.

In order to obtain a corresponding result for our analog of Hale DMO, we need only work out what the transformation of the factor $1/\nu$ is under the asymptotics that was performed to go from (6) to (9). That result is

$$\nu = \frac{\omega}{\omega_0} = \frac{t}{t_n A}. \tag{15}$$

When we introduce this multiplier on the right side of (9), we obtain,

$$u_1(x_0,\omega_0) = \frac{1}{2\pi}\int \frac{t\ dk\ dt_n}{t_n A^2}\left[1+\frac{2k^2h^2}{\omega_0^2 t_n^2}\right]U(k,t,h)\exp\{i\Theta\}. \tag{16}$$

As noted above, it is this formula and (9) that we use in our numerical test of the method to estimate the cosine of the specular angle.

Finally, we give the results for our analog of the Gardner/Forel DMO:

$$\nu = \frac{\omega}{\omega_0} = \frac{P\sqrt{4P^2+c^2t_0^2}}{hct_0} \tag{17}$$

and

$$U_1(x_0,t_0) = \sqrt{\frac{h}{2\pi c}}\int_{x_0-h}^{x_0+h}\frac{dy}{P^{3/2}}D_{1/2}[u;t]\left(c^2t_0^2+4P^2\right)^{1/4}\left[\frac{2h^2}{P^2}-1\right]. \tag{18}$$

Following our asymptotic analysis of the application of our formalism to model data, we discuss our approach to the AVO/AVA analysis. We describe possible ways for stripping away geometrical spreading effects from our peak amplitudes, so that we are left with estimates of $R(\cos\theta_S)\cos\theta_S$ and $R(\cos\theta_S)$ from our output. If we carry

out this analysis for each offset, h, for which we have data, then the result is a three column table from which to pursue AVO/AVA analysis.

In the last section, we provide a numerical example to confirm our results. We consider the reflection from a circular cylinder. For this example, we can write down the explicit formulas for the finite offset data, the zero offset data and our predicted TZO data. Then, we generate numerical data and process it with our proposed formalism. We check that the arrival times at each zero offset point are as theory requires. Furthermore, we strip away our predicted geometrical spreading effects and compare the resulting amplitude with the geometrical optics reflection coefficient of the input finite offset data. The numerical output of our processing of model data agrees with the numerical computation of theoretical prediction with less than 2% error over most of the range of model and deteriorates to 4% as end effects of the finite aperture of the model begin to take effect. Interestingly, the estimates of the cosine of the specular angle are more than an order of magnitude better, never rising to more than .1This is typical of such computations. We believe that what is happening here is that the computational errors and theoretical approximations we have made tend to "track" one another, so that the quotient has better accuracy and is smoother than either the numerator or the denominator of the quotient.

In this numerical analysis, we actually used the Hale TZO formulas, (9), (10) and (15).

TRUE AMPLITUDE TZO: DERIVATION

We describe here the derivation of a true amplitude mapping of finite offset data to zero offset data. The formalism starts from an inversion formula to map common offest data to a model and then a modeling formula to map the model to zero offset data. Thus, we begin with a brief outline of our inversion formalism.

The fundamental idea is to start with a common offset data set and write down an inversion formula for the perturbation in velocity. So, we start from the velocity representation,

$$\frac{1}{v^2} = \frac{1}{c^2}\left[1 + \alpha\right]. \tag{19}$$

In this analysis, the unknown velocity, v, and hence, the perturbation, α, as well, are functions of two spatial variables called ξ_1, ξ_3, below. The reference speed, c, is assumed to be a constant. The data set is gathered on a source/receiver array at common offset, $2h$, around a variable midpoint, y.

A symbolic representation of the formalism.

The basic idea behind our approach to the analysis is to use a cascade of two different formulas. The first of these is the inversion formula for determining α from the common offset, constant background, data set. The second is a modeling formula for determining zero offset data from an "earth model"—values of α and c. Symbolically,

then, given a data set, $u(y,\omega,h)$, we invert to find $\alpha(\xi_1,\xi_3)$ by applying an inversion operator,

$$\alpha(\xi_1,\xi_3) = \mathcal{I}_h\left[u(y,\omega,h)\right]. \tag{20}$$

In our formalism, this is an integral operator, integrating over y and ω, with a kernel that is a function of y,ω,h,ξ_1,ξ_3. In the present study, we only consider mapping from a fixed offset h to zero offset and hence suppress the $h-$dependence of the inversion operator, henceforth writing $\mathcal{I}$ instead of $\mathcal{I}_h$.

Given a solution $\alpha(\xi_1,\xi_3)$, we know how to do modeling to zero offset (or any other offset). Symbolically,

$$u_0(x_0,\omega_0) = \mathcal{M}\left[\alpha(\xi_1,\xi_3)\right]. \tag{21}$$

This is also an integral operator, integrating in the variables ξ_1,ξ_3, with a kernel that is a function of ξ_1,ξ_3,x_0,ω_0.

The cascade of these two operators produces an operator that maps $u(y,\omega,h)$ to $u_0(x_0,\omega_0)$:

$$u_0(x_0,\omega_0) = \mathcal{M}\Big[\mathcal{I}\left[u(y,\omega,h)\right]\Big]. \tag{22}$$

Note that on the right, the combined kernel of the two operators is a function of $y,\omega,h,\xi_1,\xi_3,x_0,\omega_0$ with integrations over y,ω,ξ_1,ξ_3, while *the data only depend on the variables,* y,ω,h. Thus, it is possible to simplify the operator by exploiting stationary phase to carry out the integrals in ξ_1,ξ_3, thereby greatly simplifying the resulting operation by reducing it to just integration over the variables, y,ω, that appear in the data.

The formulas that we use here for inversion and modeling are *two-and-one-half dimensional* (2.5D) formulas that are derived via perturbation theory, often called the Born approximation in the literature.

The formulas for modeling and inversion.

Here, we present the formulas for inversion and for forward modeling. We begin with the inversion formula for taking data expressed in midpoint/offset coordinates, (y,h) and producing an inversion for $\alpha(\xi_1,\xi_3)$.

$$\begin{aligned}\alpha(\xi_1,\xi_3) &= \frac{8\xi_3}{\sqrt{2\pi}c}\int dy\sqrt{r_s+r_g}\,\frac{r_s^2+r_g^2}{(r_s r_g)^{3/2}}\\ &\quad\cdot\int\frac{d\omega}{\sqrt{|\omega|}}\exp\left\{-i\omega[r_s+r_g]/c - i\pi\,\mathrm{sgn}(\omega)/4\right\}u(y,\omega,h), \qquad (23)\\ r_s &= \sqrt{(\xi_1-y+h)^2+\xi_3^2},\quad r_g=\sqrt{(\xi_1-y-h)^2+\xi_3^2};\end{aligned}$$

See Sullivan and Cohen [1987]. Some modification of their inversion result is necessary, since they provide a formula for the *reflectivity*, $\beta(\xi_1,\xi_3)$, rather than for $\alpha(\xi_1,\xi_3)$.

Next is the formula for the forward modeling of zero offset data in 2.5D using the Born approximation.

$$\begin{aligned} u(x_0,\omega_0) &= \frac{1}{16}\left[\frac{|\omega_0|}{\pi c}\right]^{3/2}\int d\xi^2\alpha(\xi_1,\xi_3)\frac{\exp\{2i\omega_0 r_0/c + i\pi\,\mathrm{sgn}(\omega_0)/4\}}{r_0^{3/2}}. \\ r_0 &= \sqrt{[\xi_1-x_0]^2+\xi_3^2}. \end{aligned} \tag{24}$$

To carry out the analysis outlined above, we cascade these two formulas to produce a formula that maps the data $u(y,\omega,h)$ to the data $u(x_0,\omega_0)$:

$$\begin{aligned} u(x_0,\omega_0) &= \frac{|\omega_0|^{3/2}e^{i\pi/4\,\mathrm{sgn}(\omega_0)}}{2^{3/2}(\pi c)^2}\int d\xi^2\frac{\xi_3}{r_0^{3/2}}\int dy\sqrt{r_s+r_g}\frac{r_s^2+r_g^2}{(r_s r_g)^{3/2}} \\ &\quad\cdot\int\frac{d\omega}{\sqrt{|\omega|}}u(y,\omega,h)\exp\{i\omega_0\Phi/c - i\pi\,\mathrm{sgn}(\omega)/4\}. \end{aligned} \tag{25}$$

In this equation,

$$\begin{aligned} \Phi &= 2r_0-\nu[r_s+r_g], \\ &= 2\sqrt{(\xi_1-x_0)^2+\xi_3^2}-\nu\left[\sqrt{(\xi_1-y+h)^2+\xi_3^2}+\sqrt{(\xi_1-y-h)^2+\xi_3^2}\right], \\ \nu &= \omega/\omega_0. \end{aligned} \tag{26}$$

Asymptotic analysis.

In our approach, the next step is to carry out the integrations in ξ_1 and ξ_3 in (25) asymptotically. When that is done, the result will be an integral operator on the data $u(y,\omega,h)$ involving integration only over y and ω to produce an expression for $u(x_0,\omega_0)$.

The condition of stationarity is that

$$\mathbf{0} = \nabla_\xi\Phi = 2\hat{r}_0 - \nu[\hat{r}_s+\hat{r}_g]. \tag{27}$$

In this equation, $\hat{r}_0$ is a unit vector from x_0 to the interior point, (ξ_1,ξ_3), and similarly for the other vectors.

The solution of equation (27) is facilitated by interpreting this equation geometrically. The vectors, $\hat{r}_0$, are normal to a circle centered at x_0. The vectors, $\nu[\hat{r}_s+\hat{r}_g]$,

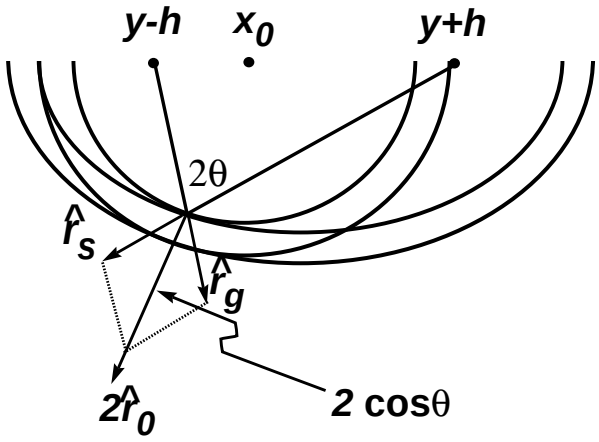

FIG. 2. A stationary point in (ξ_1, ξ_3) for given values of the variables, x_0, $y \pm h$, ω, and ω_0. The last two variables do not appear in the figure, but determine θ through the equation, $\cos\theta = \omega_0/\omega$. The ellipses have foci $y \pm h$ and the circles are centered at x_0. The smaller ellipse/circle pair satisfies the stationary phase condition on opening angle, while the larger pair does not, nor do any other ellipse/circle pair with the same foci and center.

are normal to an ellipse with foci, $y \pm h$. Both of these normals face downward. Thus, no stationary point can exist unless

$$\nu > 0, \quad \text{sgn}(\omega) = \text{sgn}(\omega_0). \tag{28}$$

Consequently, the ω-domain of integration will be restricted below to the half line on which ω has the same sign as ω_0. For the complementary domain, the integral is asymptotically of lower order in ω_0 and, presumably, smaller.

Returning to the geometry, a known fact about the normal to the ellipse is that its extension across the axis of the ellipse passes between the foci. (To confirm this, simply draw the rays from the foci to the ellipse and realize that the normal passes between them.) Equation (27) states that the two normals must be colinear. Thus, the normal to the circle centered at x_0 must also pass through the axis between the two foci.[3] Therefore, no stationary point exists unless

$$y - h < x_0 < y + h,$$

or, equivalently,

$$x_0 - h < y < x_0 + h.$$

In this latter form, this condition becomes a constraint on the domain of integration in y. When there is no stationary point, the asymptotic expansion of (25) will be of lower order in ω and, again, presumably, smaller. Thus, we neglect the complementary part of the domain of the y-integration, below.

[3]Note that the reflector that "produced" the data arising from this point shares its tangent with the circle as well as with the ellipse. For zero offset, this "normal" ray is the specular ray, as well.

Now, we can confirm these geometrical results analytically. First, take the dot product in (27) with $\hat{r}_s$ and then with $\hat{r}_g$ to conclude that

$$\hat{r}_0 \cdot \hat{r}_s = \hat{r}_0 \cdot \hat{r}_g;$$

that is, $\hat{r}_0$ makes equal angles with $\hat{r}_s$ and $\hat{r}_g$. Call that angle θ. Since, the sum, $\hat{r}_s + \hat{r}_g$, lies along the normal, note that the opening angle between the rays is just 2θ. By equating magnitudes in (27), one finds that

$$2 = 2|\hat{r}_0| = \nu|[\hat{r}_s + \hat{r}_g]| = 2\nu\cos\theta. \tag{29}$$

From the first and the last of these, and from (26) we find that

$$\frac{1}{\nu} = \frac{\omega_0}{\omega} = \cos\theta. \tag{30}$$

So, to find stationary points as functions of $y, h, x_0, \omega, \omega_0$, proceed as follows. Fix ω to be on the half line where $\mathrm{sgn}(\omega) = \mathrm{sgn}(\omega_0)$. Draw the confocal ellipses and circles. On each ellipse, pick out the points where $\cos\theta = \omega_0/\omega$ and check if the normal points back to x_0. When it does, that is a stationary value of (ξ_1, ξ_3).

Remark

> Suppose that there is nonzero data at $y + h$ at the time, $t = (r_s + r_g)/c$. In the geometrical optics limit, that data could only have arisen from a reflector sharing its tangent with some point on the ellipse, $r_s + r_g = c\,t$ Thus, the ellipse is the envelope of all of the candidate specular points at the travel time t.

Stationary values.

We need more detail about the stationary values of the variables in order to evaluate the integral (25) asymptotically. Figure 3 will be useful in explaining the determination

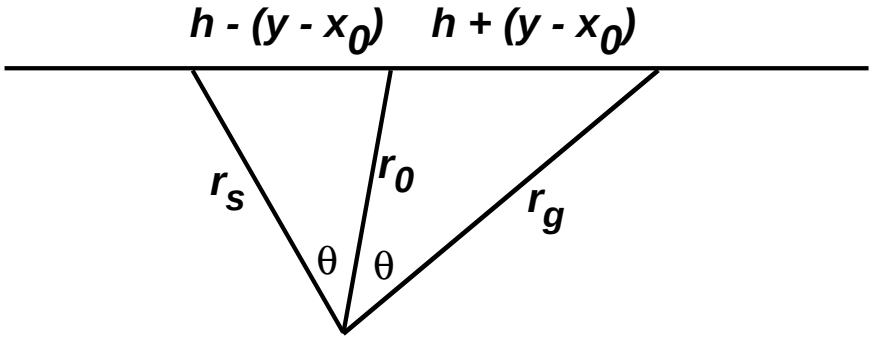

FIG. 3. Triangles relating lengths when the stationary phase conditions are satisfied.

of the variables we need. Note first the three laws of cosines associated with these triangles at stationarity:

$$\begin{aligned} 4h^2 &= r_s^2 + r_g^2 - 2r_s r_g \cos 2\theta \\ (h + (y - x_0))^2 &= r_g^2 + r_0^2 - 2r_g r_0 \cos\theta, \\ (h - (y - x_0))^2 &= r_s^2 + r_0^2 - 2r_s r_0 \cos\theta. \end{aligned}$$

Also, note that from the law of sines applied to the two smaller triangles,

$$\frac{r_s}{h - (y - x_0)} = \frac{r_g}{h + (y - x_0)}.$$

Here we have used the fact that the angles opposite the sides of length r_s and r_g are supplementary and, hence, have the same sign.

By using this result in the first law of cosines above, we can obtain a single equation for r_s or r_g and solve. In doing so, we use the relationship, (30). We find that

$$r_s = \frac{\nu h[h - (y - x_0)]}{p}, \quad r_g = \frac{\nu h[h + (y - x_0)]}{p}. \tag{31}$$

In this equation, p is given by (7). We can then use the second or third law of cosines above to find r_0: [4]

$$r_0 = \frac{h^2 - (y - x_0)^2}{p} = \frac{P^2}{p}, \tag{32}$$

with P defined by (7). Now, we can evaluate Φ in (26). We denote this stationary value by Φ_0. The result is

$$\Phi_0 = -2p, \tag{33}$$

as stated in (7).

We need to compute the Hessian of the phase, as well; that Hessian is just the Jacobian of the derivatives in (27). A nonzero Hessian implies the validity of the 2D stationary phase approximation and it also guarantees that if a solution to (27) exists, it is (locally) unique, as well. That is good enough for us!

Direct calculation of those derivatives at the stationary point yields

$$\begin{aligned} \frac{\partial^2\Phi}{\partial\xi_1^2} &= \xi_3^2\left[\frac{2}{r_0^3} - \nu\left\{\frac{1}{r_s^3} + \frac{1}{r_g^3}\right\}\right], \\ \frac{\partial^2\Phi}{\partial\xi_1\partial\xi_3} &= -\xi_3\left[\frac{2(\xi_1 - x_0)}{r_0^3} - \nu\left\{\frac{\xi_1 - y + h}{r_s^3} + \frac{\xi_1 - y - h}{r_g^3}\right\}\right], \\ \frac{\partial^2\Phi}{\partial\xi_3^2} &= \frac{2(\xi_1 - x_0)^2}{r_0^3} - \nu\left\{\frac{(\xi_1 - y + h)^2}{r_s^3} + \frac{(\xi_1 - y - h)^2}{r_g^3}\right\}. \end{aligned} \tag{34}$$

[4] Actually, we used both equations to eliminate the term linear in r_0 and solved a single linear equation for r_0^2.

By direct calulation, we find that the determinant of the matrix of second derivatives is given by

$$\begin{aligned} \text{Det}\left[\frac{\partial^2\Phi}{\partial\xi_i\partial\xi_j}\right] &= \frac{2\nu\xi_3^2}{r_s^3 r_g^3 r_0^3}\psi, \\ \psi &= 2\nu h^2 r_0^3 - (x_0 - y - h)^2 r_g^3 - (x_0 - y + h)^2 r_s^3. \end{aligned} \tag{35}$$

There is no need to evaluate the multiplier of ψ any further, since its square root (which appears in the stationary phase formula) will cancel a corresponding factor in the amplitude of (25). A simplification of ψ, itself, follows directly from the determinations of r_s and r_g in (31) and r_0 in (32). The result is

$$\psi = -2\nu h^2 P^4/p. \tag{36}$$

We note here that ψ is negative; hence, the determinant of the matrix of second derivatives is negative. This means that the eigenvalues of this matrix are of opposite sign and the signature of the matrix is equal to zero; we need this fact for evaluation of (25) by the method of stationary phase. When we carry out that evaluation, we obtain (6).

The singularity of the integrand in TZO.

The endpoint singularity of the integrand in (6) at $y = x_0 \pm h$ is only apparent. In these limits, the frequency domain integral is zero, as well, to sufficiently high order to make the integral convergent. This is difficult to show directly; however, we offer the following plausibility argument.

In the limits in question, the phase, $2\omega_0\Phi_0/c \approx -2\omega_0\nu h/c = -2\omega h/c$, and the frequency domain integral is approximately a Fourier transform of filtered data[5] at the time $2h/c$. This is the direct arrival time between source and receiver. As part of the underlying high frequency assumption, it is necessary that the reflectors of interest be "many" (at least three) wavelengths away from the source receiver line. Hence, the upward scattered data from reflectors is zero for time near $2h/c$, the arrival time of the direct wave from source to receiver. That is, the ω-integral is zero when evaluated at this time and there is no contribution from the region near the endpoints in the y-integration.

Hale DMO.

For Hale DMO, we need to express $u_0(x_0, \omega_0)$ in terms of the observed data in the (k, t)-domain. As noted in the Introduction, to derive that result from (6), we

[5]We note in passing that the filter here, $|\omega| = [(-i\omega)(i\text{sgn}(\omega)]$ represents the causal Hilbert transform of the first derivative of the data.

substitute (8) into (6) leading to the representation,

$$u_0(x_0,\omega_0) = \frac{h^2}{2\pi^2 c}\int_{x_0-h}^{x_0+h} dy \int_{\nu\geq 1} d\omega\, \nu \exp\{i\omega_0\Phi_0/c\} \cdot \left[\frac{2h^2}{P^2}-1\right]\int dk dt U(k,t,h)\exp\{i(ky+\omega t)\}. \quad (37)$$

Now the data does not depend on ω or y and those two integrals can be carried out by the method of stationary phase. The calculation is straightforward, although tedious. The result is given in equations (9) and (10).

In this form, with the data described in the (k,t)-domain, note that $t_n = 0$ corresponds to $t = 2h/c$. Thus, both the term in square brackets and the denominator, A, have singularities in this limit with the net singularity being a simple zero in the denominator. However, the data is stated explicitly in terms of t here and, as noted above, the reflected data is zero over an interval of time extending beyond $2h/c$. Hence, we need not concern ourselves about the singularity of the amplitude. In practice, instead of trying to separate out the reflected data from direct arrivals, data is merely muted to a time beyond $2h/c$.

Note, however, that the data in (9) is not expressed in terms of the same time variable as the integration is. To remedy this, we rewrite

$$U(k,t,h) = \bar{U}(k,t_n,h) \quad (38)$$

and then rewrite (9) as

$$u_0(x_0,\omega_0) = \frac{1}{2\pi}\int \frac{dk dt_n}{A}\left[1+\frac{2k^2h^2}{\omega_0^2 t_n^2}\right]\bar{U}(k,t_n,h)\exp\{i\Theta\}. \quad (39)$$

This transformation of the data amounts to *NMO processing*, that is, transformation to a time that recognizes hyperbolic moveout or time delay for a constant background trace over a horizontal reflector.

True amplitude version of Gardner and Forel's DMO

Now, we describe the derivation of the result, (11). We begin, again, with our fundamental TZO formula, (6), and take the inverse Fourier transform from the output frequency variable, ω_0 to the output time variable, t_0, defined by

$$U_0(x_0,t_0) = \frac{1}{2\pi}\int_{-\infty}^{\infty} u_0(x_0,\omega_0)\exp\{-i\omega_0 t_0\}d\omega_0. \quad (40)$$

By applying this inverse transform to (6), we obtain the following representation for our TZO formalism:

$$U_0(x_0,t_0) = \frac{h^2}{\pi c}\int d\omega_0 \int_{x_0-h}^{x_0+h} dy \int_{\nu\geq 1} d\omega\, \nu \exp\{i\omega_0\Phi/c\}\cdot\left[\frac{2h^2}{P^2}-1\right]\cdot\frac{u(y,\omega,h)}{p^2}. \quad (41)$$

In this equation,

$$\Phi = \Phi_0 - t_0, \tag{42}$$

with $\Phi_0 = -2p$ defined by (7). Again, the stationary phase analysis is fairly straightforward, with one exception. It is tedious to treat $\omega_0 p$, appearing in the definition of the phase, as a product of two functions of ω_0. Instead, we write

$$\omega_0 p = \mathrm{sgn}(\omega_0)\sqrt{\omega^2 h^2 - \omega_0^2 P^2},$$

with P defined in (7). With this bit of care in the definition of the phase, the calculation of the first and second derivatives of the phase can be carried out and the stationary value of ω_0 can be determined. Application of the stationary phase formula yields the result stated in the introduction.

This completes the derivation of the basic true amplitude TZO formula (6) and its equivalent Hale, (9) and Gardner/Forel (11) forms.

MODELING

In this section, we describe the modeling data that we intend to use to demonstrate the validity of the TZO processing formula (6). We start with Kirchhoff modeling data for finite offset between source and receiver in a constant background medium. This representation of the upward scattered field may be found in a number of sources, including Bleistein [1986] and Sullivan and Cohen [1987]. Adapted to the present example and notation, this result is

$$u_S(y,\omega,h) = \sqrt{\frac{\pi|\omega|}{c}}\frac{e^{3\pi i \mathrm{sgn}(\omega)/4}}{16\pi^2}F(\omega)\int \frac{R(\cos\theta_I)\exp\{2i\omega L/c\}}{\sqrt{r_+ r_-}\sqrt{L}}\,\hat{\boldsymbol{n}}\cdot[\hat{\boldsymbol{r}}_+ + \hat{\boldsymbol{r}}_-]ds. \tag{43}$$

Here, $F(\omega)$ is the source signature. The other relevant variables in this equation are shown in Figure 4; they are defined as follows.

- s is arclength along the curve defining the reflector in-plane.
- $\hat{\boldsymbol{n}}$ is the upward unit normal on the reflector.
- $r_\pm$ are distances between the receiver and source points, $y \pm h$, respectively, and the scattering point on the reflector, $\boldsymbol{x}(s)$:

  $$r_\pm = \sqrt{[x(s) - (y \pm h)]^2 + [z(s)]^2} \tag{44}$$

  and

  $$L = [r_+ + r_-]/2. \tag{45}$$

- The unit vectors, $\hat{\boldsymbol{r}}_\pm$ point from the surface points to the point on the reflector (downward).

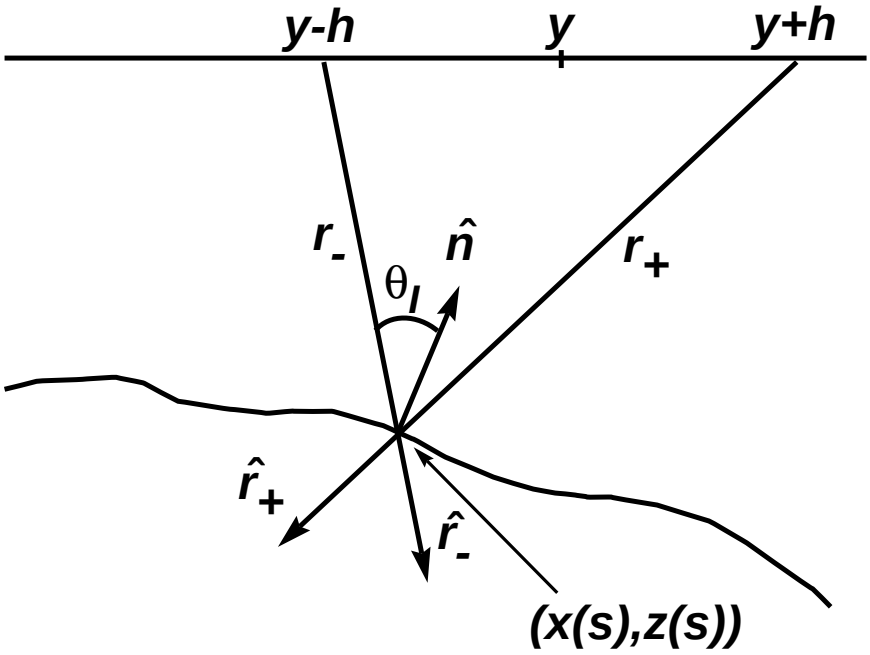

FIG. 4. Reflection geometry for the curved reflector.

- The angle, θ_I is the incidence angle of the ray from the source to the reflector, measured with respect to the normal to the reflector. Note that this is not yet the specular angle; that is, the angle with the reflected ray is not yet equal to θ_I. That only occurs for the stationary value of s, as will be seen below.
- Finally, R is the geometrical optics reflection coefficient,

$$R(\cos\theta_I) = \frac{\cos\theta_I/c - \sqrt{1/c_+^2 - 1/c^2 + \cos^2\theta_I/c^2}}{\cos\theta_I/c + \sqrt{1/c_+^2 - 1/c^2 + \cos^2\theta_I/c^2}} \tag{46}$$

with

$$\cos\theta_I = -\hat{\boldsymbol{n}}\cdot\hat{\boldsymbol{r}}_+ > 0. \tag{47}$$

For future reference, here is the result, (43), specialized to the case of zero offset:

$$u_0(x_0,\omega_0) = \sqrt{\frac{\pi|\omega|}{c}}\frac{e^{3\pi i \mathrm{sgn}(\omega)/4}}{8\pi^2}F(\omega)\int \frac{R(\cos\theta_I)\exp\{2i\omega r_0/c\}}{r_0^{3/2}}\hat{\boldsymbol{n}}\cdot\hat{\boldsymbol{r}}_0\, ds. \tag{48}$$

In this equation, the variables are as follows.

- x_0 is the zero offset surface coordinate; it is y of (43) for the case, $h = 0$.
- r_0 is the distance between the source/receiver point $(x_0, 0)$ and the scattering point on the reflector, $(x(s), y(s))$

$$r_0 = \sqrt{[x(s) - x_0]^2 + [z(s)]^2}. \tag{49}$$

- The unit vector $\hat{\boldsymbol{r}}_0$ points from the surface point to the point on the reflector (downward).
- R and θ_I are as above in (46) and (47). Here, the requirement of a distinction between θ_I and the specular angle is more apparent, the specular angle for this case will be *zero*.

The WKBJ Model.

We now show how to derive ray-theoretic data from the Kirchhoff approximate model data, (43) through (47). The point of doing this is that it will allow us to compare the zero offset ray theoretic data with the output of our processing formula applied to Kirchhoff data. We derive these modeling results by applying the method of stationary phase to the integral in (43). The phase in question is

$$\Phi(s) = 2L = r_+ + r_-, \tag{50}$$

with first derivative,

$$\dot{\Phi} = (\hat{\boldsymbol{r}}_+ + \hat{\boldsymbol{r}}_-) \cdot \dot{\boldsymbol{x}}. \tag{51}$$

In this equation we use an over-dot to denote differentiation with respect to the arclength, s. The unit vectors, $\hat{\boldsymbol{r}}_\pm$, point from the surface points $y \pm h$, respectively, to the point $\boldsymbol{x}(s)$ on the reflector. See Figure 6.

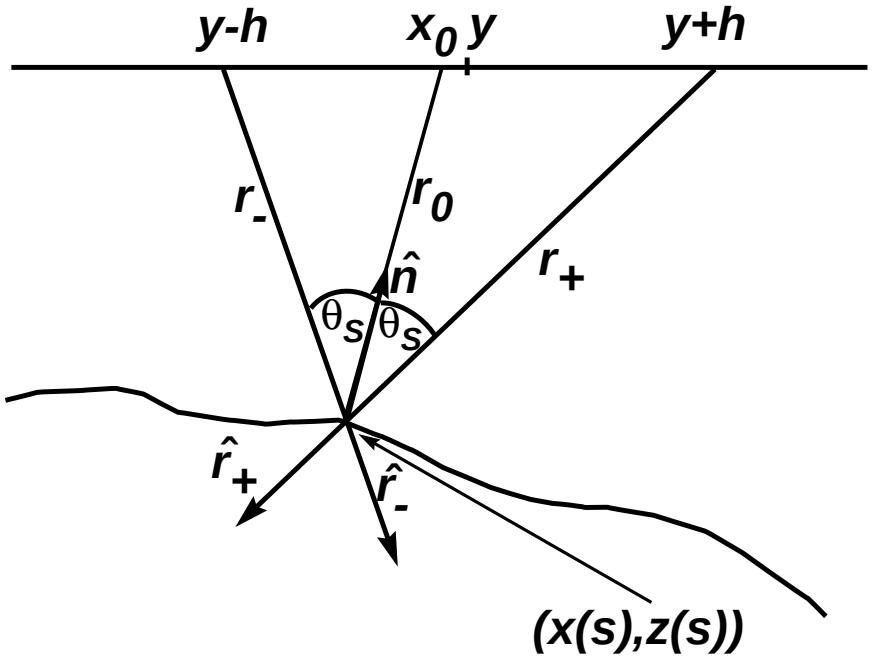

FIG. 5. Geometry relating $r_\pm$ to the zero offset distance, r_0.

The phase is stationary when $\dot{\Phi}$ is zero. This condition requires that $\hat{\boldsymbol{r}}_+ + \hat{\boldsymbol{r}}_-$ be orthogonal to the tangent to the curve at the choice of s that makes the phase

stationary. Since these are unit vectors, it is necessary that they make equal angles with the normal vector, $\hat{\boldsymbol{n}}$. We denote by θ_S this stationary value or *specular* value of θ_I. Recall that this vector was an upward-pointing normal, while $\hat{\boldsymbol{r}}_\pm$ point downward. Thus, this opening angle is just $\pi - \theta_S$ and

$$\hat{\boldsymbol{r}}_+ + \hat{\boldsymbol{r}}_- = -2\hat{\boldsymbol{n}} \cos\theta_S. \tag{52}$$

See Figure 5.

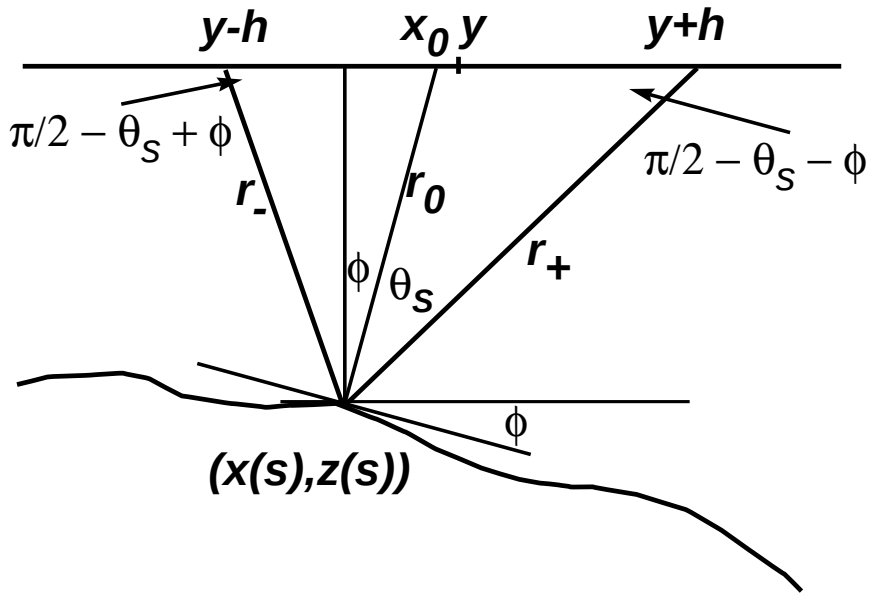

FIG. 6. The dip angle ϕ.

Define ϕ as the dip angle of the tangent to the reflector. (See Figure 6.) Then, use the law of sines to conclude that

$$\frac{r_\pm}{\sin(\pi/2 \mp \phi)} = \frac{r_0}{\sin[\pi/2 - (\theta_S \pm \phi)]}, \tag{53}$$

from which it follows that

$$\frac{1}{r_\pm} = \frac{\cos(\theta_S \pm \phi)}{r_0 \cos\phi}, \quad \frac{1}{r_+} + \frac{1}{r_-} = \frac{2\cos\theta_S}{r_0}. \tag{54}$$

These identities allow us to relate the travel distance (or travel time) for any nonzero offset specular pair of rays to the travel distance (or travel time) of the corresponding zero offset ray through use of the specular incidence angle and the dip of the reflector.

Let us now consider the second derivative of Φ which we can calculate from (51):

$$\ddot{\Phi} = (\hat{\boldsymbol{r}}_+ + \hat{\boldsymbol{r}}_-) \cdot \ddot{\boldsymbol{x}} + (\dot{\hat{\boldsymbol{r}}}_+ + \dot{\hat{\boldsymbol{r}}}_-) \cdot \dot{\boldsymbol{x}}. \tag{55}$$

In this equation, $\ddot{\boldsymbol{x}} = \boldsymbol{\kappa}_R$ is just the *curvature vector* of the reflector at the stationary point. This vector is normal to the reflector curve and points towards the convex side of the curve. By using the result (52), we find that

$$(\hat{\boldsymbol{r}}_+ + \hat{\boldsymbol{r}}_-) \cdot \ddot{\boldsymbol{x}} = -2\hat{\boldsymbol{n}} \cdot \boldsymbol{\kappa_R} \cos\theta_S = 2\mu \cos\theta_S/\rho_0. \tag{56}$$

In this last equation,

$$1/\rho_0 = |\boldsymbol{\kappa_R}|, \qquad \mu = \mathrm{sgn}(-\hat{\boldsymbol{n}} \cdot \boldsymbol{\kappa_R}). \tag{57}$$

Now consider the second term in (55). We calculate the derivative as follows.

$$\hat{\boldsymbol{r}}_\pm = \frac{\boldsymbol{r}_\pm}{r_\pm} \quad , \quad \dot{\hat{\boldsymbol{r}}}_\pm = \frac{\dot{\boldsymbol{x}}}{r_\pm} - \frac{\hat{\boldsymbol{r}}_\pm \cdot \dot{\boldsymbol{x}}}{r_\pm^3}\dot{\boldsymbol{x}} \Rightarrow$$

$$\begin{aligned}
\dot{\hat{\boldsymbol{r}}}_\pm \cdot \dot{\boldsymbol{x}} &= \frac{1}{r_\pm} - \frac{(\dot{\hat{\boldsymbol{r}}}_\pm \cdot \dot{\boldsymbol{x}})^2}{r_\pm^3} \\
&= \frac{1}{r_\pm}\left[1 - \cos^2(\pi/2 \mp \theta_S)\right] \\
&= \frac{\cos^2\theta_S}{r_\pm}
\end{aligned}$$

Here, we have used the fact that $\hat{\boldsymbol{r}}_\pm$ make angles $\pi \mp \theta_S$ with the normal and therefore

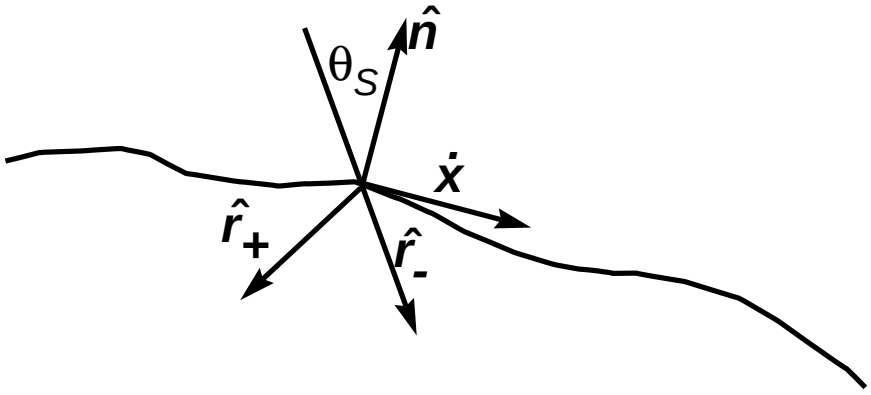

FIG. 7. Tangent vector at the stationary point.

make angles $\pi/2 \mp \theta_S$ with the tangent, $\dot{\boldsymbol{x}}$. See Figure 7.

We are now prepared to use these results to calculate the second derivative, (55):

$$\ddot{\Phi} = 2\frac{\mu \cos\theta_S}{\rho_0} + \cos^2\theta_S \left[\frac{1}{r_+} + \frac{1}{r_-}\right]$$

$$= 2\cos\theta_S \left[\frac{\mu}{\rho_0} + \frac{\cos^2\theta_S}{r_0}\right] \tag{58}$$

$$= 2\mu\cos\theta_S \left[\frac{r_0 + \mu\rho_0\cos^2\theta_S}{r_0\rho_0}\right].$$

We also calculate

$$\begin{aligned}\frac{1}{\sqrt{r_+ r_-}\sqrt{r_+ + r_-}} &= \sqrt{\frac{r_+ + r_-}{r_+ r_-}} \cdot \frac{1}{r_+ + r_-} \\ &= \sqrt{\frac{1}{r_+} + \frac{1}{r_-}} \cdot \frac{1}{r_+ + r_-} \\ &= \sqrt{\frac{2\cos\theta_S}{r_0}} \cdot \frac{1}{r_+ + r_-}.\end{aligned}$$

Remark

Actually, the second term in (55) has a nice interpretation in terms of curvature, as well. To see this, let us define $c\,t$ to be the value of $r_+ + r_-$ at the stationary point and consider the curve,

$$r_+ + r_- = c\,t,$$

that is, the *isochron* through the stationary point. The normal to the isochron always makes equal angles with the rays from the source and receive to any point on the isochron. In particular, at stationarity, these rays are just the specular rays and the normal to the isochron is in the same direction as the normal to the reflector. Of course, then, the same is true for the tangents to the two curves at that point; that is, the isochron and the reflector are tangent at the stationary point.

Let σ denote arclength on the isochron and take the second derivative of the equation of the isochron above to find that

$$(\hat{\boldsymbol{r}}_+ + \hat{\boldsymbol{r}}_-)\cdot\boldsymbol{x}'' + (\hat{\boldsymbol{r}}'_+ + \hat{\boldsymbol{r}}'_-)\cdot\boldsymbol{x}' = 0 \quad \Rightarrow \quad (\hat{\boldsymbol{r}}'_+ + \hat{\boldsymbol{r}}'_-)\cdot\boldsymbol{x}' = -(\hat{\boldsymbol{r}}_+ + \hat{\boldsymbol{r}}_-)\cdot\boldsymbol{x}''$$

Here, $'$ denotes differentiation with respect to σ. However, we know that $\boldsymbol{x}' = \dot{\boldsymbol{x}}$ since they represent two unit tangents.[6] It is a fairly straightforward computation to show that

$$\begin{aligned}\hat{\boldsymbol{r}}'_\pm \cdot \boldsymbol{x}' &= \frac{1}{r_\pm}\left[1 - (\hat{\boldsymbol{r}}_\pm \cdot \boldsymbol{x}')^2\right] \\ &= \frac{1}{r_\pm}\left[1 - (\hat{\boldsymbol{r}}_\pm \cdot \dot{\boldsymbol{x}})^2\right] \\ &= \dot{\hat{\boldsymbol{r}}}_\pm \cdot \dot{\boldsymbol{x}},\end{aligned}$$

[6]With no loss of generality, we have taken the orientations of s and σ to agree.

where the last two lines are valid at the stationary point, only. Note that this allows us to represent the right term in (55) in terms of the second derivative along the isochron:

$$(\dot{\hat{\boldsymbol{r}}}_+ + \dot{\hat{\boldsymbol{r}}}_-) \cdot \dot{\boldsymbol{x}} = -(\hat{\boldsymbol{r}}_+ + \hat{\boldsymbol{r}}_-) \cdot \boldsymbol{x}'' = 2\hat{\boldsymbol{n}} \cdot \boldsymbol{\kappa_I} \cos\theta_S$$

Here, we use $\boldsymbol{\kappa_I}$ to denote the curvature of the isochron at the reflection point. When we use this result for the second term in (55) and use (56) for the first term, we obtain the result

$$\ddot{\Phi} = 2\hat{\boldsymbol{n}} \cdot [\boldsymbol{\kappa_I} - \boldsymbol{\kappa_R}] \cos\theta_S.$$

This is the form that Tygel, etal., [1995a, 1995b, 1997] use in their analysis. As noted in the introduction, this leads to different, but equivalent representations of the upward scattered wave from the one we prefer for the discussion here.

We now have all of the constituents of the integral representation of the upward scattered wave, equation (43). After some algebra, we find that

$$u(y,\omega,h) = -e^{i\gamma}\frac{F(\omega)R(\cos\theta_S)}{8\pi L}\sqrt{\frac{|\mu\rho_0\cos^2\theta_S|}{|r_0+\mu\rho_0\cos^2\theta_S|}}\exp\{2i\omega L/c\}. \tag{59}$$

In this equation,

$$L = (r_+ + r_-)/2, \quad \gamma = \mathrm{sgn}(\omega)\left[\frac{3\pi}{4} + \frac{\pi}{4}\mathrm{sgn}(\ddot{\Phi})\right]; \tag{60}$$

all quantities must be evaluated at the stationary point where the unit vectors, $\hat{\boldsymbol{r}}_\pm$, make equal angles θ_S with $\hat{\boldsymbol{n}}$. If there is more than one such point, then the wave field is the sum of all such contributions. On the other hand, this result is invalid when $\ddot{\Phi} = 0$ at the stationary point. For $\mu > 0$, which occurs when the reflector is convex *downward* or anticlinal at the stationary point, one can verify from the second line in (58) that $\mathrm{sgn}(\ddot{\Phi}) = +1$ and $-\exp\{-i\gamma\} = +1$.

In the phase of this result, $2L/c = (r_+ + r_-)/c$ is just the travel time on the ray path connecting the source and receiver with the specular point on the reflector. In the amplitude, the factor, $1/[8\pi L] = 1/[4\pi(r_+ + r_-)]$ should be recognized as the geometrical spreading effect for a planar reflector with the same dip angle as the curved reflector at the specular point. The factor, $\sqrt{\{|\mu\rho_0\cos^2\theta_S|/(|r_0+\mu\rho_0\cos^2\theta_S|)\}}$, is a geometrical spreading effect specifically due to the curvature of the reflector. Note that as the specular point moves towards a point where the reflector is planar, $\rho_0 \to \infty$, and this second factor approaches unity. In this manner, the geometrical spreading for the curved reflector reduces to that of the planar reflector in this limit. The equation of a reflector dipping at angle ϕ, is given by

$$(x - x_e)\sin\phi - z\cos\phi = 0, \tag{61}$$

where x_e is the emergence point of the dipping plane, and, consistent with our "righthanded" (x, z)-coordinate system, ϕ is measured positively in a clockwise rotation from the positive $x-$axis. (Thus, in particular, $\phi > 0$ in Figure 6). For this case x_e is assumed to be far enough to the left so that the specular point is "many" (at least three!) wavelengths below the observation point y, and $y - h$ is many wavelengths to the right of x_e.

The limiting form of (59) for the dipping planar reflector is

$$u(y, \omega, h) = \frac{R(\cos\theta_S)\exp\{2i\omega L/c\}}{8\pi L}, \tag{62}$$

with

$$L = \sqrt{(y - x_e)^2 \sin^2\phi + h^2\cos^2\phi}. \tag{63}$$

Also, one can show that, in this limit, the specular angle θ_S is determined by[7]

$$\cos\theta_S = \frac{(y - x_e)\sin\phi}{L}. \tag{64}$$

We can further find the limit for a horizontal plane by allowing $\phi \to 0\pm$ and $x_e \to \mp\infty$ in such a manner that

$$-x_e \sin\phi \to H,$$

where H is the depth of the horizontal planar reflector. In that case u is again given by (62), except that now,

$$L = \sqrt{H^2 + h^2}, \quad \cos\theta_S = h/L. \tag{65}$$

The zero offset limit of the result, (59), is also worth noting. Here, the incidence angle is zero; the zero offset ray lies along the normal to the reflector and (59) becomes

$$u(y, \omega, 0) = -e^{i\gamma}\frac{F(\omega)R_n}{8\pi r_0}\sqrt{\frac{|\mu\rho_0|}{|r_0 + \mu\rho_0|}}\exp\{2i\omega r_0/c\}. \tag{66}$$

In this equation, we have introduced R_n for the normal incidence reflection coefficient,

$$R_n = \frac{c_+ - c}{c_+ + c}. \tag{67}$$

Furthermore, the effect of curvature $\sqrt{|\mu\rho_0|}/(|r_0 + \mu\rho_0|)$, lends itself to an easy interpretation. The distance along the normal from the specular point to the center of

[7]It is also possible to obtain a result that does not explicitly depend on x_e, namely, $\cos\theta_S = \sqrt{L^2 - h^2\cos^2\phi}/L$. The easiest way to derive this result is geometrically. In Figure 8, ahead, where there is a dipping plane, the coordinate, x_e is replaced by ξ. In that figure, form the right triangle with hypotenuse, $2L$, extend the line forming the angle θ_S above the data line and drop a perpendicular from the receiver at $y + h$ to this extended line. The expression for $\cos\theta_S$ in this triangle is exactly the result stated here.

curvature of the reflector-curve is given by ρ_0. This is the numerator of the fraction here. The denominator is the distance from the center of curvature to the observation point. This ratio measures the change in the arclength of a differential circular arc centered at the center of curvature, with the numerator being the arclength at the specular point and the denominator being the arclength at the observation point.

Also, it is easier here to interpret the condition that $\ddot{\Phi} = 0$. This can only occur for $\mu = -1$, and, as noted above, the reflector curve must be convex-upward or synclinal at the specular point. Furthermore, it is necessary that $r_0 = \rho_0$; that is, the observation point must be right at the center of curvature. This is the situation when the "buried focus" is right at the observation surface.

To complete the story of ray theoretical or geometrical optics model data, we specialize the zero offset results to the planar dipping reflector as

$$u(y, \omega, 0) = \frac{F(\omega) R_n}{8\pi r_0} \exp\{2i\omega r_0/c\}. \tag{68}$$

Here,

$$r_0 = L = (y - x_e) \sin\phi, \tag{69}$$

from (63) and R_n is given by (67). Finally, for the horizontal reflector, $r_0 = L = H$ and

$$u(y, \omega, 0) = \frac{F(\omega) R_n}{8\pi H} \exp\{2i\omega H/c\}. \tag{70}$$

Returning to the nonzero offset case (59), once more, we see that the effect of curvature is still expressed in terms of the distance to the zero offset point (r_0) except that now the *effective* radius of curvature in this factor is $\rho_0 \cos^2\theta_S$.

Thus, we see the analysis of a "true amplitude TZO" amounts to determining the extent to which the nonzero offset wavefield, (59), is transformed into the zero offset wavefield (66). As noted in the Introduction, it is known from earlier results that the proposed processing formulas preserve the finite offset reflection coefficient while the planar finite offset geometrical spreading effect and travel time are transformed to the zero offset counterparts. The new result to be shown here is that the finite offset curvature effect is mapped to its zero offset counterpart.

A PRELIMINARY RESULT

Below, we will apply the processing formula (6) to the Kirchhoff approximate model data for a curved reflector, (43). However, we will first apply the processing formula to the dipping planar data, (62–64), because it provides us with some results that we will need for the more difficult case of the curved reflector.

In both cases, we will proceed by applying the method of stationary phase to the double integral in y and ω appearing in (6). Examination of the model data in (43) and (62) reveals that the dependence of the phase in both is simply linear in ω. The

details of the differences in these two modeling formulas only arise when we carry out the y-integration. Thus, it is worthwhile to carry out the stationary phase analysis in ω for both cases as a canonical integral. That integral is

$$\mathcal{I}(\eta) = \int_{\nu>1} |\omega|^{\eta} \nu p^{-2} F(\omega) d\omega \exp\{2i\omega_0 \Psi/c\}, \tag{71}$$

with the phase here being the sum of phases in the model data, $2\omega L/c$ and in the TZO processing operator (6), $2\omega_0 p$; that is,

$$\Psi = \nu L - p, \quad \nu = \omega/\omega_0. \tag{72}$$

Below, we will need this result for $\eta = 0$ in the application of our formalism to geometrical optics data and for $\eta = 1/2$ in the application of our formalism to Kirchhoff approximate data.

The purpose of this section is to derive the asymptotic expansion of the integral $\mathcal{I}(\eta)$ for high frequency, that is, for the "large" parameter[8], $2\omega_0/c$. Thus, we first write down the two derivatives,

$$\frac{\partial \Psi}{\partial \omega} = \frac{1}{\omega_0}\left[L - \frac{\nu h^2}{p}\right], \qquad \frac{\partial^2 \Psi}{\partial \omega^2} = \frac{h^2 P^2}{\omega_0^2 p^3} > 0, \tag{73}$$

for nonzero offset h and for y bounded away from the endpoints $x_0 \mp h$. In this equation, P is defined by (7).

Setting the first derivative equal to zero yields the following solution for ν, with a corresponding solution, $\omega = \omega_0 \nu$:

$$\nu = \frac{L}{h}\frac{P}{Q}, \tag{74}$$

with

$$Q = \sqrt{L^2 - h^2}. \tag{75}$$

By using this value of ν in (7), we find that

$$p = \frac{hP}{Q} \tag{76}$$

and then from (72) and (73) we find that

$$\Psi = PQ/h, \quad \frac{\partial^2 \Psi}{\partial \omega^2} = \frac{Q^3}{\omega_0^2 h P}. \tag{77}$$

[8]Technically, we should identify a dimensionless large parameter which would be this wave number multiplied by a "typical" length scale of the problem. The most natural length scale of the problem for this purpose is the range to the reflector. Thus, $2\omega_0 r_0/c$ would serve as an appropriate large dimensionless parameter. However, we know that if we carry out our analysis formally in dimensional variables, the final result will be the same as if we were to transform the problem entirely to dimensionless variables, do asymptotics, and then return to the dimensional variables of the original problem. Thus, we do not bother with this intermediary transformation and simply proceed formally in dimensional variables.

We use the results above and the standard stationary phase formula for a simple stationary point to find that to leading order

$$\mathcal{I}(\eta) = \sqrt{\frac{\pi c|\omega_0|}{PQ}}\frac{L}{h^{5/2}}\left[\frac{PL}{hQ}\right]^{\eta} F(\nu\omega_0)\exp\{2i\omega_0 PQ/(hc) + i\pi\mathrm{sgn}(\omega_0)/4\}. \tag{78}$$

Thus, for the case, $\eta = 0$, this result becomes

$$\mathcal{I}(0) = \sqrt{\frac{\pi c|\omega_0|}{PQ}}\frac{L}{h^{5/2}}F(\nu\omega_0)\exp\{2i\omega_0 PQ/(hc) + i\pi\mathrm{sgn}(\omega_0)/4\}, \tag{79}$$

and for the case $\eta = 1/2$,

$$\mathcal{I}(1/2) = \sqrt{\pi c|\omega_0|}\frac{L^{3/2}}{Qh^3}F(\nu\omega_0)\exp\{2i\omega_0 PQ/(hc) + i\pi\mathrm{sgn}(\omega_0)/4\}. \tag{80}$$

As noted above, in the following sections, these integrals will arise in the asymptotic analysis of the application of the TZO processing formula (6) to model data for the dipping plane and the curved reflector.

APPLICATION OF TZO TO REFLECTION DATA FROM A DIPPING PLANE

We consider now the case of a dipping reflector at dip angle ϕ as shown in Figure

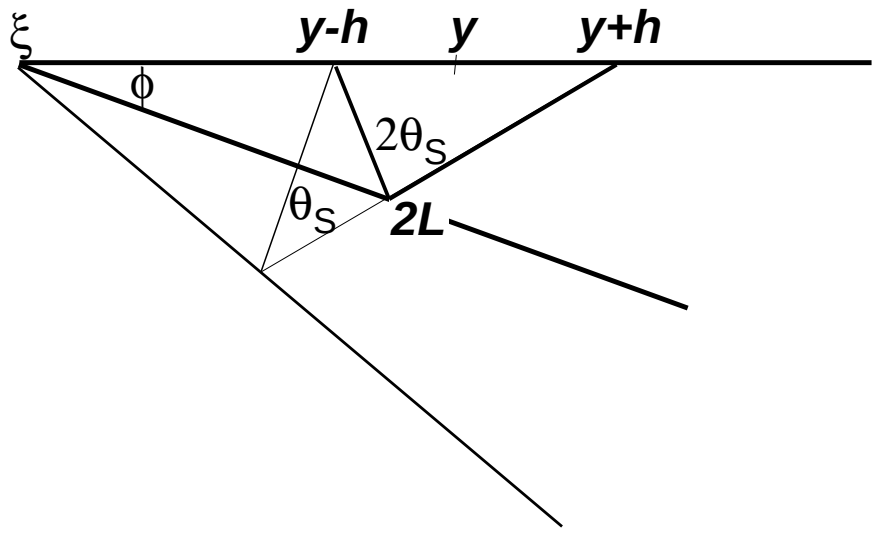

FIG. 8. Reflection geometry for the dipping reflector.

8. This result has been presented earlier [Bleistein, 1990]. However, the results of this

analysis will prove key to the stationary phase analysis of the processing for model data for the curved reflector in the next section.

The model data for this case is given by (62 – 64). When this representation is substituted into (6), the resulting integral representation for u_0 becomes

$$u_0(x_0,\omega_0) = \frac{h^2}{8\pi^2 c}\int_{x_0-h}^{x_0+h}\mathcal{I}(0)\,dy\left[\frac{2h^2}{P^2}-1\right]\frac{R(\cos\theta_S)}{L}. \tag{81}$$

Here, $\mathcal{I}(0)$ is defined by (71) and its asymptotic expansion is given by (79), with P defined by (7) and Q defined by (75), except that for this geometry, Q can be further simplified to

$$Q = \sin\phi\sqrt{(y-\xi)^2-h^2}. \tag{82}$$

By using this asymptotic expansion in (81) above, we find that

$$\begin{aligned} u_0(x_0,\omega_0) &= \sqrt{\frac{|\omega_0|}{\pi c h}}\frac{e^{i\pi \mathrm{sgn}(\omega_0)/4}}{8\pi} \\ &\quad\cdot\int_{x_0-h}^{x_0+h}dy F(\omega_0 LP/hQ)\frac{R(\cos\theta_S)}{\sqrt{PQ}}\left[\frac{2h^2}{P^2}-1\right]\exp\{2i\omega_0\Psi/c\}, \end{aligned} \tag{83}$$

with Ψ given in (77) and ν given in (74).

We can now proceed to carry out the method of stationary phase in the variable y. The derivatives of the phase, Ψ, (77), are given by

$$\begin{aligned} \frac{\partial\Psi}{\partial y} &= \frac{1}{h}\left[-\frac{(y-x_0)Q}{P}+\frac{P(y-\xi)\sin^2\phi}{Q}\right], \\ \frac{\partial^2\Psi}{\partial y^2} &= -\frac{1}{h}\left[\frac{Qh^2}{P^3}+\frac{Ph^2\sin^4\phi}{Q^3}+2\frac{(y-x_0)(y-\xi)\sin^2\phi}{PQ}\right]. \end{aligned} \tag{84}$$

Setting the first derivative of Ψ equal to zero and solving for y yields the following set of results

$$\begin{aligned} y-\xi &= \frac{(x_0-\xi)[\sqrt{1+4h^2/(x_0-\xi)^2}+1]}{2}, \\ y-x_0 &= \frac{(x_0-\xi)[\sqrt{1+4h^2/(x_0-\xi)^2}-1]}{2}, \end{aligned} \tag{85}$$

$$(y-\xi)^2 = (x_0-\xi)(y-\xi)+h^2, \quad (y-x_0)^2 = -(x_0-\xi)(y-x_0)+h^2,$$
$$P^2 = (x_0-\xi)(y-x_0), \quad Q^2 = (x_0-\xi)(y-\xi)\sin^2\phi, \quad PQ = (x_0-\xi)h\sin\phi,$$

$$r_0 = (x_0 - \xi)\sin\phi.$$

With these results, we are able to determine that

$$\Psi = x_0 \sin\phi, \qquad \frac{\partial^2\Psi}{\partial y^2} = -\frac{((x_0-\xi)^2 + 4h^2)\sin^2\phi}{PQ} < 0. \tag{86}$$

Furthermore, one can verify that,

$$\nu = \sec\theta_S, \tag{87}$$

with θ_S being the specular value associated with the output zero offset point x_0:

$$\cos^2\theta_S = \frac{[x_0 - \xi + \sqrt{(x_0-\xi)^2 + 4h^2}]\sin^2\phi}{\sqrt{(x_0-\xi)^2 + 4h^2} - (x_0 - \xi)\cos 2\phi}; \tag{88}$$

see Figure 9.

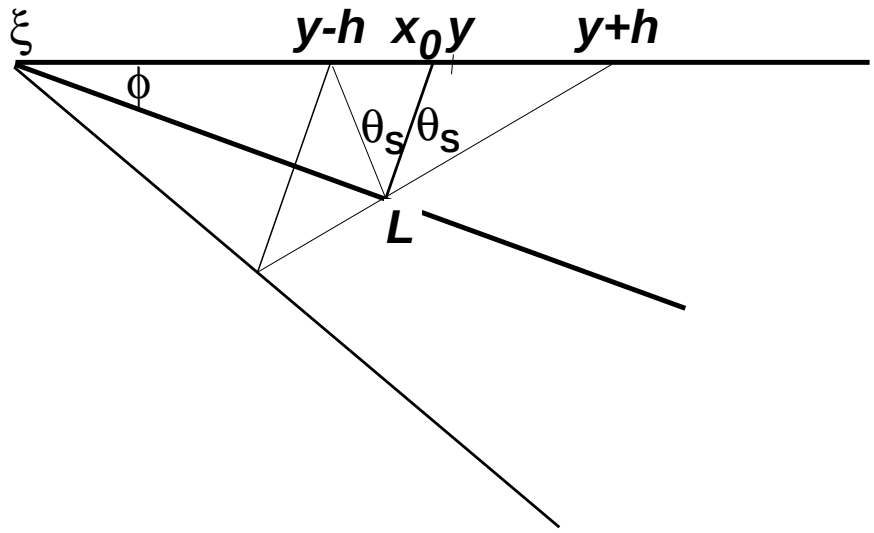

FIG. 9. Dip geometry with x_0 and y coupled by the stationary phase condition.

With these values substituted into (81), we obtain the following result:

$$u_0(x_0,\omega_0) = \frac{R(\cos\theta_S)F(\omega_0\sec\theta_S)\exp\{2i\omega_0 r_0/c\}}{8\pi r_0}. \tag{89}$$

This result fits our prediction in the Introduction. Finite offset and geometrical spreading have been replaced by their zero offset counterparts. The reflection coefficient at the finite offset specular angle associated with x_0 is preserved in the amplitude and the bandwidth of the source signature is again scaled by $\cos\theta_S$. Note that θ_S varies with x_0. However, we propose determining the specular value of $\cos\theta_S$ by the same method as is used for determining $\cos\theta_S$ in our inversion formalism.

Estimating $\cos\theta_S$.

We can now contemplate repeating this analysis for the operator $u_1(x_0,\omega_0)$, defined by (14). However, we really only need to compare this operator and (6) to know how to extract that result from (89), above. Since the operators differ by a factor of ν, the outputs will differ by the stationary value of ν determined by (87), above, namely, $\sec\theta_S$. Then, the ratio of the two outputs yields an estimate of the value of $\cos\theta_S$. This is the motivation for the second operator, (14), in the introduction. As noted there, the second operator in the alternative TZO formulas was derived by determining the stationary value of ν under the transformations of (6) to the alternative input and/or output variables.

This ratio is most easily extracted when the data is transformed back to the time domain. There, reflection events are seen as peaks along the trace and one need only take the ratio of peak values to obtain the desired result. This method will not work at points on the trace where there are crossing events.

APPLICATION TO REFLECTION DATA FROM A CURVED REFLECTOR.

In this section we describe the results of applying the TZO processing formula, (6), to the Kirchhoff model data for a curved reflector, (43). It is here that we verify the new result that the geometrical spreading factor in the reflected wave for finite offset data is replaced by the corresponding factor for zero offset data under the transformation that we propose. We use (43) rather than (59) because in the latter result, the specular variables are only defined implicitly in terms of y and the parametric curve representing the reflector. We find it easier to work with this representation in which all variables are given explicitly.

When the data, (43), is substituted into (6), the resulting integral representation for $u_0(x_0,\omega_0)$ is

$$\begin{aligned} u_0(x_0,\omega_0) &= \frac{h^2}{(4\pi)^2}\sqrt{\frac{2}{\pi c^3}}\int_{x_0-h}^{x_0+h}dy\left[\frac{2h^2}{P^2}-1\right] \\ &\quad\cdot\int ds\mathcal{I}(1/2)\frac{R(\cos\theta_I)\,\hat{n}\cdot(\hat{r}_+ + \hat{r}_-)}{\sqrt{r_+ r_-}\sqrt{L}}. \end{aligned} \tag{90}$$

Here, $\mathcal{I}(1/2)$ is defined by (7) and its asymptotic expansion with respect to ω_0 is given by (80).

When (80) is substituted into (90) above, the result is

$$u_0(x_0,\omega_0) = -\frac{|\omega_0|}{(4\pi)^2 ch\sqrt{2}}\int_{x_0-h}^{x_0+h}dy\int ds F(\omega_0 LP/hQ) \tag{91}$$

$$\cdot \left[\frac{2h^2}{P^2} - 1\right] \frac{L}{Q} \frac{R(\cos\theta_I)\,\hat{n}\cdot(\hat{r}_+ + \hat{r}_-)}{\sqrt{r_+ r_-}} e^{2i\omega_0 \Psi/c}.$$

In this equation, L is defined by (44) and (45); P is defined by (7); Q is defined by (75); finally,

$$\Psi = PQ/h = \sqrt{h^2 - (y - x_0)^2}\sqrt{L^2 - h^2}/h. \tag{92}$$

We now proceed to stationary phase in the variable y. The first derivative of the phase, Ψ, (92), is given by

$$\frac{\partial \Psi}{\partial y} = \frac{1}{h}\left\{-\frac{(y - x_0)Q}{P} + \frac{PL}{2Q}\left[\frac{y + h - x(s)}{r_+} + \frac{y - h - x(s)}{r_-}\right]\right\}. \tag{93}$$

We need to find the value of y that makes this derivative equal to zero for given values of x_0 and s. The key to doing this is to use the dipping plane case as a model. There, we were able to find a solution in terms of the dip angle of the plane. Here, we artificially introduce an appropriate plane[9] and then use the same solution. The trick is in introducing the "right" plane. To do so, proceed as follows. Draw the line connecting the points, $(x_0, 0)$ and $(x(s), z(s))$ and draw the plane perpendicular to this line through the latter point. See Figure 10.

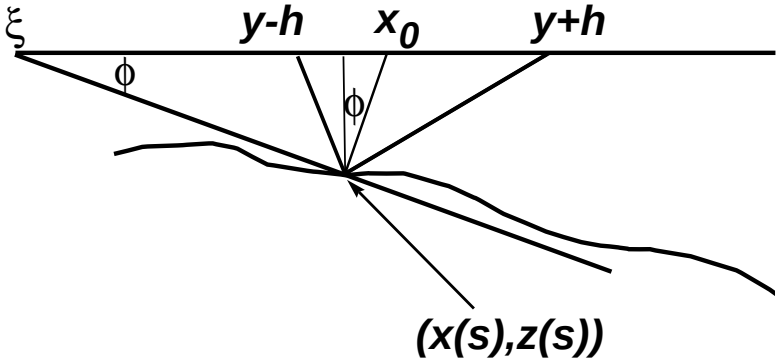

FIG. 10. Artificial plane used to find the stationary value of y.

The dip angle ϕ for this plane is just the inclination with respect to the vertical of the drawn line:

$$\sin\phi = \frac{x_0 - x(s)}{r_0}, \qquad \cos\phi = \frac{z(s)}{r_0}, \tag{94}$$

$$r_0 = \sqrt{(x_0 - x(s))^2 + z^2(s)}.$$

[9]Note that we speak of "plane" here, even though our computation is two dimensional, rather than three dimensional. Recall that this is 2.5D processing, in which we have assumed no out-of-plane variations. Thus, we have reduced the 3D problem to a 2D computation, totally within the $(x, z)-$plane. Therefore, we speak of a planar reflector, but carry out all of our analysis with respect to lines in the vertical plane in which the out-of-plane coordinate is evaluated at zero. (Indeed, we have used y for the in-plane midpoint coordinate of the common offset data set.)

This plane intersects the upper surface at the point

$$\xi = x(s) + \frac{z^2(s)}{x(s) - x_0}; \quad x_0 - \xi = -\frac{r_0^2}{x_0 - x(s)}. \tag{95}$$

We can now read off our solution and constituent variables from the results in (85). Thus, we find that

$$y - \xi = \frac{x_0 - \xi}{2} \cdot \left[\sqrt{1 + 4h^2/(x_0 - \xi)^2} + 1\right] \tag{96}$$

and

$$y - x_0 = \frac{x_0 - \xi}{2} \cdot \left[\sqrt{1 + 4h^2/(x_0 - \xi)^2} - 1\right]. \tag{97}$$

In addition, one can derive the following results:

$$\begin{aligned}
y - \xi &= \frac{\csc\phi}{2}\left[\sqrt{r_0^2 + 4h^2\sin^2\phi} + r_0\right], \\
y - x_0 &= \frac{\csc\phi}{2}\left[\sqrt{r_0^2 + 4h^2\sin^2\phi} - r_0\right], \\
L^2 &= (y-\xi)^2\sin^2\phi + h^2\cos^2\phi = \frac{r_0}{2}\left[\sqrt{r_0^2 + 4h^2\sin^2\phi} + r_0\right] + h^2, \\
Q^2 &= L^2 - h^2, \quad P^2 = \frac{r_0\csc^2\phi}{2}\left[\sqrt{r_0^2 + 4h^2\sin^2\phi} - r_0\right].
\end{aligned} \tag{98}$$

Note that ϕ has been defined to be positive for x_0 to the right of $x(s)$ and ϕ is negative for x_0 to the left of $x(s)$. Thus, the sign of $y - \xi$ and $y - x_0$ is determined by the sign of ϕ in the first two equations here.

From these results, one can check that

$$(y - x_0)Q^2 = r_0 h^2 \sin\phi \tag{99}$$

by direct substitution. To verify that the derivative in (93) is zero, we must compare this result with the expression

$$\frac{P^2 L}{2}\left[\frac{y + h - x(s)}{r_+} + \frac{y - h - x(s)}{r_-}\right]. \tag{100}$$

To calculate this expression in terms of the same variables, r_0, ϕ and h, we start first with the following identity that arises from the appropriate triangles in Figure 11 being similar:

$$\begin{aligned}
\frac{L}{r_\pm} &= \frac{(y \pm h - \xi)\sin\phi}{r_0} \\
&= \frac{1}{r_0}\left[\frac{\sqrt{r_0^2 + 4h^2\sin^2\phi} + r_0}{2} \mp h\sin\phi\right].
\end{aligned} \tag{101}$$

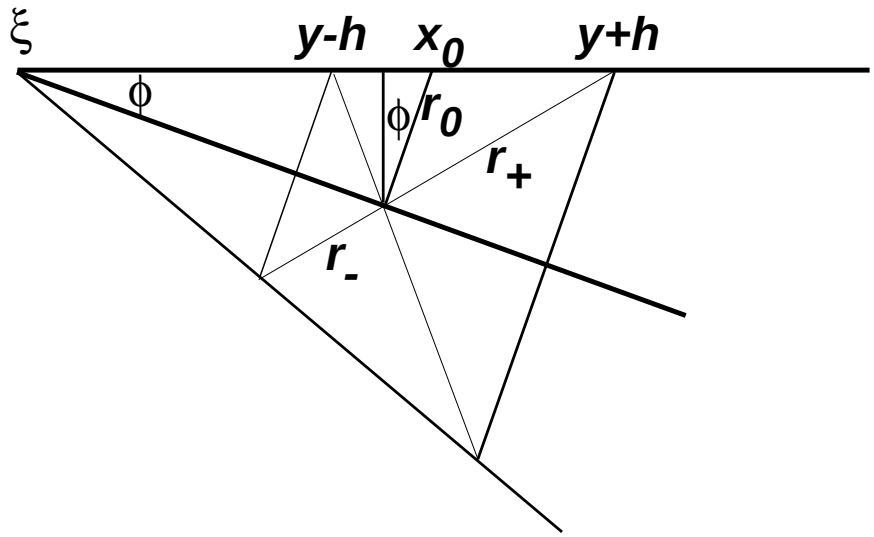

FIG. 11. The dipping plane, with $r_\pm$, r_0, and ϕ shown. Note that $2L = r_+ + r_-$ and the diagonals parallel to the line of length r_0 have lengths $2(y \pm h - \xi)\sin\phi$.

Now, one needs only to carry out the computations indicated in (100) using (98) to confirm that the right side of (99) is obtained for that expression, as well. With those two expressions being equal, we have confirmed that the solution, (96), makes $\partial\Psi/\partial y$ zero.

One can now confirm that

$$\Psi = r_0. \tag{102}$$

From (101) and (98), one can verify that

$$r_+ r_- = \frac{r_0 L^2}{Q^2}. \tag{103}$$

Other useful identities follow from these results. For example, one can use (64) and (98) to find that

$$\cos\theta_I = \frac{\sqrt{r_0^2 + 4h^2\sin^2\phi} + r_0}{2L}. \tag{104}$$

Note that θ_I in this case, *is* the specular angle for the synthetically created dipping planar reflector here. We reserve the notation, θ_S, for the final specular angle of the curved reflector. Since the planar reflector, pointwise, is not yet the tangent plane to the reflector, these two angles are not equal.

It is easy to check now that

$$\nu = \sec\theta_I \tag{105}$$

by substituting into (74). Furthermore, referring to the amplitude in (91), we now compute

$$\frac{2h^2}{P^2} - 1 = \frac{\sqrt{r_0^2 + 4h^2\sin^2\phi} + r_0}{r_0}. \tag{106}$$

Furthermore,

$$\hat{n} \cdot (\hat{r}_+ + \hat{r}_-) = 2 \cos\theta_I \hat{n} \cdot \hat{r}_0. \tag{107}$$

Let us now turn to the analysis of the second derivative of the phase, (92). Differentiation of (93) yields the result,

$$\begin{aligned} \frac{\partial^2 \Psi}{\partial y^2} &= -\frac{1}{h}\left\{ \frac{Qh^2}{P^3} + \frac{(y-x_0)L}{PQ}\left[\frac{y+h-x_s}{r_+} + \frac{y-h-x_s}{r_-}\right] \right. \\ &\quad + \frac{Ph^2}{4Q^3}\left[\frac{y+h-x_s}{r_+} + \frac{y-h-x_s}{r_-}\right]^2 \\ &\quad \left. - \frac{PLz_s^2}{2Q}\left[\frac{1}{r_+^3} + \frac{1}{r_-^3}\right]\right\}. \end{aligned} \tag{108}$$

Here, we have used the results

$$\frac{P}{Q} - \frac{PL^2}{Q^3} = \frac{P}{Q^3}\left[Q^2 - L^2\right] = -\frac{Ph^2}{Q^3}, \tag{109}$$

to simplify the expression for the second derivative. The last equality arises from the definition of Q in (75).

The evaluation of the second derivative at stationarity was carried out with the aid of *Mathematica*. For the reader who wishes to check the result below, we provide some of the intermediary results.

$$\frac{Qh^2}{P^3} = \frac{1}{r_0 h}\left[\frac{r_0}{2}\left[\sqrt{r_0^2 + 4h^2\sin^2\phi} + r_0\right] + h^2\sin^2\phi\right]$$

$$\begin{aligned} \frac{(y-x_0)L}{PQ}\left[\frac{y+h-x_s}{r_+} + \frac{y-h-x_s}{r_-}\right] &= \frac{2h\sin^2\phi}{r_0} \\ \frac{Ph^2}{4Q^3}\left[\frac{y+h-x_s}{r_+} + \frac{y-h-x_s}{r_-}\right]^2 &= \frac{h^3\sin^2\phi}{r_0 L^2} \end{aligned}$$

$$-\frac{PLz_s^2}{2Q}\left[\frac{1}{r_+^3} + \frac{1}{r_-^3}\right] = -\frac{h\cos^2\phi}{2L^2}\left[\sqrt{r_0^2 + 4h^2\sin^2\phi} + r_0\right] - \frac{4h^3}{r_0 L^2}\cos^2\phi\sin^2\phi.$$

Mathematica also effectively combines these terms to yield the final result,

$$\frac{\partial^2 \Psi}{\partial y^2} = -\frac{\left[r_0^2 + 4h^2\sin^2\phi\right]\left[\sqrt{r_0^2 + 4h^2\sin^2\phi} + r_0\right]^2}{2h^2 r_0 L^2}. \tag{110}$$

We now have all of the pieces necessary to evaluate u_0 in (91). The result is

$$u_0(x_0,\omega_0) = \sqrt{\frac{\pi|\omega_0|}{c}}\frac{e^{3\pi i/4}\mathrm{sgn}(\omega_0)}{8\pi^2}\int F(\omega_0\sec\theta_I)\frac{R(\cos\theta_I)e^{2i\omega_0 r_0/c}}{r_0^{3/2}}\hat{\boldsymbol{n}}\cdot\hat{\boldsymbol{r}}_0 ds. \tag{111}$$

This result should be compared to the zero offset result (48), which is the Kirchhoff representation for the zero offset data. We see that the two results are the same except for the replacement,

$$F(\omega) \to F(\omega_0 \sec\theta_I), \tag{112}$$

and the meaning of θ_I. In (48), this is the incident angle that the ray from $(x_0, 0)$ to $\boldsymbol{x}(s)$ makes with the normal at the latter point. Here, θ_I is the angle between the ray from $(y-h, 0)$ and $\boldsymbol{x}(s)$ and the ray from $(x_0, 0)$ to $\boldsymbol{x}(s)$, which is the incidence angle of the offset ray with respect to the normal to the artificially constructing reflecting plane at $\boldsymbol{x}(s)$.

We can now further simplify this result by carrying out the same stationary phase analysis as was done in the discussion starting with (50). However, there is no need to redo the calculations; we need only understand the implications of the replacements we have just noted. At specular, the ray $(x_0, 0)$ to $\boldsymbol{x}(s)$ is normal to the surface, in which case the θ_I appearing in this formula is the incidence angle that the specular offset source/receiver pair makes with the reflector. The choice of y for each x_0 is given by (98), where we must interpret r_0 as the normal distance from x_0 to the reflector and ϕ as the dip angle of the tangent at that normal incidence point. Of course, if there is more than one normal from x_0 to the reflector—that is, more than one stationary point in s— u_0 is a sum of contributions from all of the stationary points. This was true in (98), as well.

Recall that the question at issue here was whether or not the finite offset curvature effect was mapped to the zero offset curvature effect by the TZO operator. We can now answer that question in the affirmative. From this point forward, the stationary phase analysis proceeds as it would for zero-offset Kirchhoff modeling, with the curvature effect in the integral in (111) arising solely from the evaluation of the second derivative of r_0 with respect to s. Since this analysis is exactly the same as for the true Kirchhoff modeling, (55–58), we can immediately read off the result of applying stationary phase in s to (111) from the result (66). The result is

$$u_0(x_0, \omega_0) = -e^{i\gamma}\frac{F(\omega_0 \sec\theta_S)R(\cos\theta_S)}{8\pi r_0}\sqrt{\frac{|\mu\rho_0|}{|r_0+\mu\rho_0|}}e^{2i\omega_0 r_0/c}. \tag{113}$$

In this equation, θ_S is given by (104) subject to the additional constraint that $\hat{\boldsymbol{r}}_0$ must be normal to the reflector.

Estimating $\cos\theta_S$.

We have now identified θ_I with θ_S at stationarity. Furthermore, as part of our asymptotic analysis, we have the result (105) that identifies ν with θ_I. Combining these observations allows us to conclude that at the peak value of the reflection response, the second TZO operator, (14), will produce the amplitude of the first operator, (6), scaled by $\sec\theta_S$. As discussed in the previous section, the ratio of the outputs yields an estimate of $\cos\theta_S$.

What we have shown.

We characterize this result as follows.

1. The angularly dependent reflection coefficient of the finite offset specular source/-receiver pair associated with the zero offset point, x_0 is preserved.

2. The bandwidth of the source signature is scaled by $\cos\theta$ and the source signature itself is compressed into this smaller range through the scaling of argument by $\sec\theta$.

3. The finite offset geometrical spreading effect, $1/(r_+ + r_-)$, has been replaced by the zero offset geometrical spreading effect, $1/2r_0$.

4. *The finite offset curvature effect of the input signal has been replaced by the zero offset curvature effect.*

It is this last feature that required this asymptotic analysis and was the motivation for this study.

In addition, we have shown that by the simple expedient of simultaneously processing two outputs, we can obtain an estimate of the specular angle associated with the preserved specular reflection coefficient in the TZO output.

AMPLITUDE VERSUS OFFSET OR ANGLE.

Here, we discuss the possibility of using our true amplitude TZO processing for AVO/AVA analysis. For this analysis, we consider the predictions of our asymptotic analysis when we apply our operators to data from a single reflector. In (5), we have already provided the expression for the peak value, U_{0PEAK}. From our earlier discussion, we know that the peak value, U_{1PEAK} will just be that result multiplied by $\sec\theta_S$:

$$U_{1PEAK} = \frac{R(\cos\theta_S)}{8\pi r_0}\sqrt{\frac{\rho_0}{r_0+\rho_0}}\int F(\omega)d\omega. \tag{114}$$

As noted previously, the ratio of the outputs provides an estimate of $\cos\theta$:

$$\frac{U_{0PEAK}}{U_{1PEAK}} = \cos\theta_S. \tag{115}$$

Thus, we can contemplate generating a table of values of $\cos\theta$ as a function of h by applying our processing, (6) and (14) to data at each offset.

Now, let us examine the result, (114), above, with an eye towards extracting the value of R, itself, from this result. We observe, first, that for our constant background model, $r_0 = ct_{0PEAK}$, with this time being the time at which the peak value on the trace is observed. Furthermore, let us assume that we know the source signature. If the reflector were planar, the curvature factor would be replaced by unity and only

the reflection coefficient would be left as an unknown on the right side of the equation. Hence, we could solve for the reflection coefficient at each offset. This would allow us to fill in a third column of our table, yielding $\cos\theta_S$ and $R(\cos\theta_S)$ as functions of h.

Now consider the curved reflector. We now have the additional problem of determining the factor arising from curvature in the peak amplitude in (114). A significant aspect of the result of our earlier analysis is that, no matter the offset of the input data, after processing, *the curvature effect on the output data is independent of the offset of the input data.* Thus, if we could determine the curvature dependent factor for some particular offset, we would know it for all offsets. We propose two possible ways to do this. Firstly, the normal incidence reflection coefficient might be known from other analysis. Secondly, note, again, that the only factor in (114) that varies with offset is the reflection coefficient. Thus, from a plot of the output agains offset, one might be able to recognize the critical offset, that is the offset corresponding critical incidence in the reflection coefficient. At this point, the reflection coefficient is equal to unity and the only unknown in (114) is the curvature factor. Once this factor is determined from critical incidence, it is know for all incidence angles or all offsets. Hence, again, we can determine $(\cos\theta_S)$ to fill in the third column of our table.

In summary, without knowing anything about the geometry of the reflector or the location of the reflection point that produces an event on the input trace, TZO processing of data at all offsets allows the possibility of determining the reflection coefficient as a function of offset or incidence angle.

NUMERICAL TEST

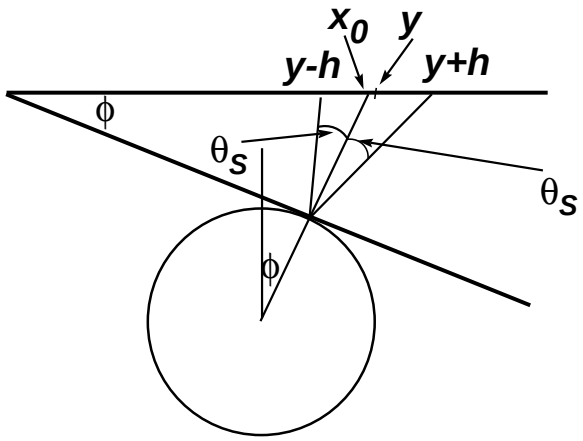

FIG. 12. Geometry for the circular reflector model.

Here, we will test our method on a synthetic data example. We consider a reflector that is a circular cylinder, with center at depth 2km, radius, 1 km. See Figure 12. We generate synthetic common offset data with $2h = 1km$, velocity, 1km/s above the reflector, 4km/s below the reflector, and process the synthetic data with the formula,

(6). This result should agree with (3). We take the Fourier transform to the time domain and check the peak location of the output against the zero offset time, $2r_0/c$, predicted in (3). The match is virtually exact.

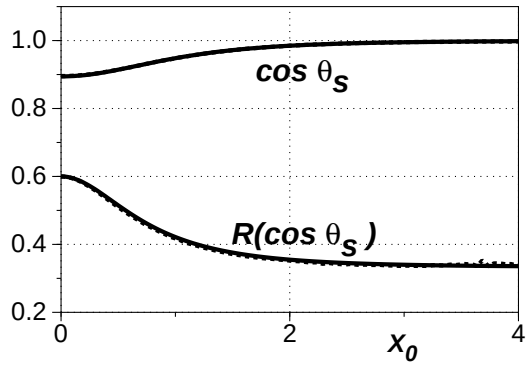

FIG. 13. Comparison of theoretical (solid curve) results and and computed (dashed curve) results for both the reflection coefficient of the TZO output (lower curve) and $\cos\theta_S$ (upper curve) as a function of x_0, the zero offset output coordinate.

Next, we take the amplitude at this peak value divide it by the area under the frequency domain filter of the source, accounting for the factor of $\sec\theta_S$ appearing in (3). Furthermore, we extract the geometrical spreading effects apparent in that formula. All that remains is the reflection coefficient. In the lower curve of Figure 13 we plot the reflection coefficient against x_0 (dashed curve) and the theoretical reflection coefficient (solid curve). The two are seen to agree extremely well out to about 3km, beyond which, endpoint effects, due to the finite aperture of the model data, begin to degrade the results.

To estimate the cosine of the specular incidence angle, $\cos\theta_S$, we take the quotient of peak amplitudes, U_{0PEAK}/U_{1PEAK}, from equations (5) and (114). The results are shown in the upper curve in in Figure 13. Here, the agreement is visually even better; we can almost not distinguish the theoretical and computed values.

We remark that this last result does not depend on using a true amplitude formalism. For any DMO, simply compute two outputs where the integrands differ by the appropriate multiplier—(15), for Hale DMO; (17), for Gardner/Forel DMO—and the quotient will yield an estimate of $\cos\theta_S$. Note, also, the smoothness of this output. We conclude that the numerical errors of the two computations apparently "track" one another and do not show up in the quotient.

Finally, in Figure 14, we plot the relative errors of the two computations. One can see, here, that the error in the estimate of reflection coefficient is less that 2% out to 3km and peaks at 4% between 3 and 4km. The estimate of $\cos\theta$ is more than an order of magnitude better over this entire range, not even degrading where the estimate of reflection coefficient does—beyond 3km. The maximum error is less than .1rise to

1coefficient is so large—40%—as to render the output meaningless for this esimate. This region is simply beyond the range of validity due to limited aperture of the model data.

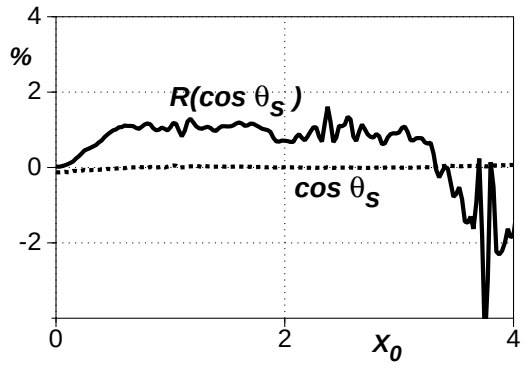

FIG. 14. Percentage error in the estimate of the reflection coefficient as a function of zero offset point (solid curve) and the percentage error in the estimate of the cosine of the specular angle (dashed curve).

Thus, with this numerical example we have provided tests that verify that the predictions of the asymptotic theory are correct.

CONCLUSIONS

We have now provided a derivation of the claims of the Introduction. It has been shown that the TZO processing proposed here in (6) transforms the amplitude and phase of the finite offset data to zero offset data, except for the reflection coefficient, whose finite offset specular value has been retained.

We have proposed a method for determining this specular angle. One need only carry two running sums in the processing, differing by a factor of ν, whose asymptotic value is $\sec\theta_S$. Thus, the quotient of the two outputs at specular provides an estimate of this factor or, equivalently, of $\cos\theta_S$.

We have also proposed a method of carrying out AVO/AVA analysis on the output traces of our processing over multiple offsets.

Finally, we provided a synthetic test of our method that produces output consistent with the theory that we have proposed.

REFERENCES

Black, J. L., Schleicher, K. L., and Zhang, L., 1993, True amplitude imaging and dip moveout: Geophysics, 58, 1, 47-66.

Bleistein, N., 1984, "Mathematical Methods for Wave Phenomena," Academic Press Inc. (Harcourt Brace Jovanovich Publishers), New York.

Bleistein, N., 1990, Born DMO revisited: 60th Annual International Meeting of the Society of Exploration Geophysicists, Expanded Abstracts, 1366-1369.

Fomel, S., 1995a, Amplitude preserving offset continuation in theory, Part 1: the offset continuation equation: Stanford Exploration Project preprint, SEP-84, 179-196.

Fomel, S., 1995b, Amplitude preserving offset continuation in theory, Part 2: solving the equation: Stanford Exploration Project preprint, SEP-89.

Fomel, S., N. Bleistein, H. Jaramillo, J. K. Cohen, 1996, True amplitude DMO, offset continuation and AVA/AVO for curved reflectors: 66th Annual International Meeting of the Society of Exploration Geophysicists, Expanded Abstracts, 1731-1734.

Gardner, Gerald H. F. and Forel, David, 1988, Amplitude preservation equations for DMO: 58th Annual Internat. Mtg., Soc. Expl. Geophys., Expanded Abstracts, 1106-1108, Session: S17.2.

Gardner, G. H. F. and Forel, D., 1995, Amplitude preservation equations for dip moveout: Geophysics, 55, 485-487.

Geoltrain, S., 1991, Automatic association of kinematic information to prestack images: 61st Annual Internat. Mtg., Soc. Expl. Geophys., Expanded Abstracts, 890-892, Session: SI1.5.

Hale, I. D., 1984, Dip-moveout by Fourier transform: Geophysics, 49, 6, 741-757.

Liner, C. L., 1990, General theory and comparative anatomy of dip moveout: Geophysics, 55, 5, 595-607.

Liner, C. L., 1991, Born theory of wave-equation dip moveout: Geophysics, 56, 2, 182-189.

Sullivan, M. F., and Cohen, J. K., 1987, Pre-stack Kirchhoff inversion of common offset data, Geophysics, 52, 745-754.

Tygel, M., Schleicher, J., and Hubral, P., 1995a, True-amplitude migration to zero offset (MZO) by diffraction stack: preprint Insitituto de Matemática Estatística e Ciência da Computação, Universidade Estadadual de Campinas, Brazil.

Tygel, M., Schleicher, J., and Hubral, P., 1995b, Dualities between reflectors and reflection time surfaces: Journal of Seismic Exploration, Vol. 4, pp. 123 - 150.

Tygel, M., Schleicher, J., Hubral, P., and Santos, L. T., 1997, 2.5-D true-amplitude Kirchhoff migration to zero offset in laterally inhomogeneous media: Geophysics, to appear.

Zhang, L., 1988, A new Jacobian for dip-moveout: Stanford Exploration Project, SEP-59, 201-208.

ACKNOWLEDGMENTS

The authors wish to acknowledge the ACTI Project, No. 4731U0015-2F, Los Alamos National Laboratory, and industry project partners in that program, as well as the Center for Wave Phenomena Consortium Project at the Colorado School of Mines for their financial support of this research. In addition, we wish to acknowledge the encouragement of Bee Bednar to pursue the Gardner/Forel version of our method.